Revision -1

Experimental study along the magnesio-hornblende–glaucophane join

by

Jie Lei[1,2], David M. Jenkins[1,*], and Kiyotaka Ishida[3]

[1]Dept. Geological Sci. and Env. Studies, Binghamton University, Binghamton, NY, 13902-6000, U.S.A.

[2]China Shenhua Overseas Development and Investment Co., Beijing, China, 100025

[3]Department of Environmental Changes, Graduate School of Social and Cultural Studies, Kyushu University, 744 Motooka, Nishi-ku, Fukuoka 819-0395, Japan

* E-mail: dmjenks@binghamton.edu

ABSTRACT

Amphiboles have played a leading role in metamorphic petrology, from helping to define several metamorphic facies to forming the basis of geothermobarometry, if their thermodynamic mixing properties can be calibrated to the temperature and pressure of formation. Compositional variations of sodium- and sodium-calcium-amphiboles may reveal important information about paleo-subduction zones but have not been studied as much as the more common calcium-amphiboles. In this study we investigate the mixing properties of amphibole solid solutions between magnesio-hornblende and glaucophane $[^{B}Ca_2{}^{C}(Mg_4Al)^{T}(AlSi_7)O_{22}(OH)_2$–$^{B}Na_2{}^{C}(Mg_3Al_2)^{T}(Si_8)O_{22}(OH)_2]$ as a binary sub-join within the ternary amphibole system tremolite–glaucophane–tschermakite where the principal substitutions are Ca for Na at the B, Al for Mg at the C, and Al for Si at the T crystallographic sites. Amphiboles were made from mixtures of reagent oxides at 10 mol% increments between magnesio-hornblende and glaucophane, formed in a piston-cylinder press at 735–860°C and 1.3–2.5 GPa for 72–216 hours giving good yields (92–100 wt%). A positive

deviation is present in the volume-composition plot, even after correcting volumes for non-binary components, supporting the presence of a positive deviation in the enthalpy of mixing (ΔH^{mix}) along this join. Fourier transform infrared spectra (FTIR) were obtained in the range of 350–4000 cm^{-1} for the mid-infrared spectra (MIR) for the purpose of estimating the extent of short-range ordering and for autocorrelation analysis, and in the 650–50 cm^{-1} for far-infrared spectra (FIR) for autocorrelation analysis. Autocorrelation analysis gave $\delta\Delta Corr$ values which further support a positive deviation in the ΔH^{mix} along the magnsio-hornblende–glaucophane join, although the $\delta\Delta Corr$ maximum did not occur at the calcium-poor (i.e., glaucophane-rich) portion of the join as expected. Synthetic end-member glaucophane and magnesio-hornblende were mixed in a molar ratio of 1:1 and allowed to equilibrate by homogenization for variable durations in the range of 600–800 °C at 2.0 GPa to determine the maximum-width of the miscibility gap. These compositional re-equilibration experiments suggested the presence of an asymmetric miscibility gap (steeper toward glaucophane) with a critical-point below 700 °C. Combining the results of this study with previously published results on the tremolite–glaucophane join allowed refinement of several asymmetric formalism mixing parameters (i.e., $W_{Gl,Ts}$ = 20 kJ, α_{Ts} = 1.2) and modeling of the miscibility gap within the tremolite–glaucophane–tschermakite ternary system. The results showed that the composition of the critical point is very close to the maximum in the autocorrelation parameter $\delta\Delta Corr$, as one would predict. An important implication of this study is that low-temperature immiscibility between calcium- and sodium-rich amphiboles may be more important than the role of pressure, as proposed by Brown (1977, J. Petrol.), in accounting for the change in B-site Na contents of metamorphic amphiboles.

Keywords: Magnesio-hornblende, Glaucophane, Miscibility-gap, Autocorrelation, Infrared spectra, Thermodynamic modeling

INTRODUCTION

Amphiboles are major rock-forming minerals in many metamorphic rocks, helping to define up to seven metamorphic facies (Liou et al. 1985; Vernon and Clarke 2008, p. 33). Their wide range of compositions offer considerable potential for deducing the pressures (*P*) and temperatures (*T*) under which a particular rock formed, as indicated by geothermobarometers that are in common use for calcium-amphiboles (e.g., Hammarstrom and Zen 1986; Schmidt 1992; Holland and Blundy 1994). Rocks rich in glaucophane [$^{A}\square^{B}Na_2^{C}(Mg_3Al_2)^{T}Si_8O_{22}(OH)_2$ = Gl, where $\square$ represents a vacancy] typically occur in blueschist-facies metamorphic terranes (e.g., Ernst 1963; Maruyama et al. 1996) so that any *P*-*T* information extracted from these amphiboles will help define the burial depths and/or geothermal gradients of the plate-convergent zones in which these rocks occur. Geothermobarometry involving sodium- or sodium-calcium-amphiboles has not been so extensively developed because of the difficulties of working experimentally with chemically-complex natural amphiboles at low temperatures (Maruyama et al. 1986) and because of the experimental challenges of working with end-member glaucophane at high temperatures (e.g., Jenkins and Corona 2006a). Recent advances in the synthesis of nearly end-member glaucophane (Jenkins and Corona 2006a) have provided opportunities for exploring basic questions about the energetics of cation mixing in sodium-rich amphiboles and, in turn, for calculating how their compositions vary with *P* and *T*.

In the survey of metamorphic amphiboles presented by Schumacher (2007), the compositions of most calcium-, sodium-calcium-, and sodium-amphiboles are comprised by the end-member compositions tremolite [$^{A}\square^{B}Ca_2^{C}Mg_5^{T}Si_8O_{22}(OH)_2$= Tr], edenite [$^{A}Na^{B}Ca_2^{C}Mg_5^{T}(AlSi_7)O_{22}(OH)_2$ = Ed], tschermakite [$^{A}\square^{B}Ca_2^{C}(Mg_3Al_2)^{T}(Al_2Si_6)O_{22}(OH)_2$ = Ts], and glaucophane. The edenite component is fairly minor in sodium-amphiboles as well

as in coexisting sodium- and calcium-amphiboles, allowing us to model closely these amphibole compositions with the ternary system tremolite, glaucophane, and tschermakite. Considerable information is available on the stability and crystal-chemistry of tremolite (Jenkins 1987; Jenkins and Clare 1990; Welch and Pawley 1991; Maresch et al. 1994; Zimmerman et al. 1996; Gottschalk et al. 1999; Evans et al. 2000, Bozhilov et al. 2007) such that the conditions needed to make synthetic tremolite, even if not of ideal stoichiometry, are well established. Tschermakite is an important component in many amphibole-based exchange reactions; unfortunately, end-member tschermakite has not been synthesized (Jasmund and Schäfer 1972; Jenkins 1988, 1994; Cho and Ernst 1991; Hoschek 1995; Najorka and Gottschalk 2003). Instead, the limit of Al solid solution appears to be close to that of magnesio-hornblende [$^{A}\square^{B}Ca_2{}^{C}(Mg_4Al)^{T}(AlSi_7)O_{22}(OH)_2$ = Hb], a composition that lies halfway between tremolite and tschermakite. Finally, nearly pure glaucophane has been synthesized by Jenkins and Corona (2006a), Corona and Jenkins (2007), Jenkins (2011), Basora et al. (2012), and Corona et al. (2013) if strict control is maintained on the water content to prevent the formation of an expandable phyllosilicate (tri-octahedral smectite) and to limit the loss of soluble constituents (e.g., Na, Al and Si) to the ambient fluid. Progress over the last two decades on the synthesis of tremolite, magnesio-hornblende, and glaucophane allows us to investigate the crystal-chemistry and energetics of cation mixing along several key compositional joins, namely, the tremolite–glaucophane join, which was recently studied by Jenkins et al. (2013, 2014), and the magnesio-hornblende–glaucophane join, the subject of this study. Together these two compositional joins provide fairly complete coverage of the compositional space relevant to sodium- and sodium-calcium amphiboles.

Synthesis of magnesio-hornblende of ideal composition has proven difficult. As with other calcium-amphiboles, there is a small but persistent tendency to have less than the theoretical value of 2 Ca and 2 Al atoms per formula unit (apfu), which has been discussed in

more detail by Cao et al. (1986), Jenkins (1988, 1994), and Najorka and Gottschalk (2003). Therefore we used a magnesio-hornblende-rich amphibole with the nominal bulk composition $^{A}\square^{B}(Ca_{1.85}Mg_{0.15})^{C}(Mg_{4.1}Al_{0.9})^{T}(Si_{7.1}Al_{0.9})O_{22}(OH)_2$, named "A". The slight depletion in Ca and Al and enrichment in Mg was chosen because of its likelihood of yielding essentially pure amphibole. Accordingly, experiments were conducted strictly along the "A"–Gl join, slightly displaced from the Hb–Gl join, to maximize amphibole yields. We stress that data extracted from the amphiboles formed in this study is based on the observed, rather than presumed or nominal compositions, to account for any compositional deviations from the intended join.

Previous studies of metamorphic amphibole (e.g., Himmelberg and Papike 1969; Ernst 1979; Maresch et al. 1982; Reynard and Ballèvre 1988; Smelik and Veblen 1992) have documented that glaucophane shares a miscibility gap or solvus, rather than having complete solid solution, with calcic amphiboles. Accordingly, a primary focus of this study is to document the location of any miscibility gap along the Hb–Gl join. One indication of the presence of a miscibility gap can be seen in the volume-composition relationships along the Hb–Gl join, where the presence of a positive deviation from ideal mixing of molar volumes supports the tendency for unmixing. We also studied amphibole dissolution or re-equilibration of two end-member amphiboles mixed in a molar ratio of 1:1 to determine the location of the critical temperature and to place constraints on the maximum size of the miscibility gap.

There has been significant effort given to analyzing the infrared (IR) spectra of synthetic amphiboles in the past several decades, primarily in the OH-stretching region of 3800–3200 cm^{-1} for the purpose of deducing short-range order (e.g., Hawthorne et al. 2000; Hawthorne and Della Ventura 2007). More recently, analysis of mineral IR spectra in the mid- and far-IR range (1200–100 cm^{-1}) using the method known as autocorrelation has provided a means for

characterizing the amount of inter-atomic strain and, therefore, the energetics associated with cation substitution within minerals (Salje et al. 2000). It is possible to use IR spectra to analyze mixing properties because the phonon spectra samples a length scale of several unit cells that contains much information about local strain associated with atomic substitutions in the lattice (Boffa Ballaran et al. 1998, 1999; Atkinson et al. 1999; Carpenter and Boffa Ballaran 2001; Tarantino et al. 2002; Carpenter 2002). Cation mixing and order/disorder within the amphibole structure can be detected by both IR peak shifts and band-width variations with changes in amphibole composition (Boffa Ballaran et al. 2001; Boffa Ballaran and Carpenter 2003). Autocorrelation is a convenient means of characterizing IR spectra that may be both complex and asymmetric in nature, using the Gaussian-based peak-width parameter $\Delta Corr$, and the relative changes in this parameter expressed as $\delta\Delta Corr$, to reveal systematic changes in band width (Salje et al. 2000). Substitutions along a solid solution join with a positive excess volume and positive elastic energy typically leads to line-broadening, which, in turn, is correlated with the enthalpy of mixing (Boffa Ballaran and Carpenter 2003; Etzel and Benisek 2008). Even if absolute values for the enthalpy of mixing cannot be derived, Jenkins et al. (2014) proposed that autocorrelation analysis should at least provide the sense of asymmetry of the enthalpy or excess Gibbs free energy of mixing along the join. Therefore, we use infrared spectra in the OH-stretching region, mid-infrared, and far-infrared range of amphiboles formed in this study to gain additional insights into the short-range order and energetics of mixing along the Hb–Gl join.

METHODS

Amphibole synthesis and apparatus:

All amphiboles were synthesized from mixtures of reagent grade oxides and carbonates (Na_2CO_3, $CaCO_3$, MgO, Al_2O_3 and SiO_2). The SiO_2 was made from silicic acid heated in

steps to 1100°C in air, yielding amorphous silica or weakly crystalline cristobalite. After weighing and mixing the reagents Na_2CO_3, $CaCO_3$, Al_2O_3 and SiO_2, they were heated at 900°C for 15 minutes to remove CO_2. Magnesium was then added as $Mg(OH)_2$ for most of the mixtures, using the hydroxide as the source of water. Only for one mixture (MgHG-1) was the $Mg(OH)_2$ mixed in before decarbonation, to which 3 wt% of distilled water was added later. The bulk compositions of all samples investigated in this study are presented in Table 1.

Starting mixtures were treated in sealed Pt capsules, which were made from tubing that was cleaned in acetone and then oven- or flame-annealed to around 1,200 °C. Pt capsules were either 4.0 mm outer diameter (OD) by 15 mm length (synthesis experiments) or 1.5 mm OD by 5.5 mm length (retreatment experiments) having wall thicknesses of 0.13–0.18 mm. A ½-inch diameter piston-cylinder press was used for all experiments with NaCl serving as the pressure medium and fitted with a straight graphite furnace. Temperatures were measured with a chromel-alumel thermocouple situated in the salt pressure media directly above the sample. The specific synthesis conditions are listed in Table 2.

Analytical equipment and methods

Powder X-ray diffraction analysis was done by grinding the samples in an agate mortar under ethanol. The powder was mounted on a zero background oriented quartz plate and analyzed by a Philips X'Pert PW3040-MPD diffractometer operated at 40 kV and 20 mA using Cu-Kα radiation fitted with a diffracted-beam graphite monochromator. All of the samples were first analyzed from 5 to 50° 2θ (short scan) with step sizes of 0.02° 2θ to see whether the sample needed a retreatment or showed no additional amphibole growth. Once the samples were confirmed to have reached their optimal yield, a step scan over the range 8 to 100° 2θ (long scan) at increments of 0.05° 2θ was done for sufficient time (2–3 sec/step) to obtain ~1000–2000 counts on the major peaks. Rietveld refinements were done using the

program GSAS (Larson and Von Dreele 2000). Reagent grade NaCl (a_0 = 5.6401 Å) was added in the samples to serve as an internal standard to adjust the zero point of the patterns. Refinements were initiated using the structure of glaucophane from Papike and Clark (1968), pargasite (for hornblende) from Sharma and Jenkins (1999), talc from Perdikatsis and Burzlaff (1981), quartz from Levien et al. (1980), and smectite using the vermiculite structure of Shirozu and Bailey (1966). The following parameters were adjusted during refinements of the long scans in the sequence indicated: (1) zero point relative to NaCl, but held constant there after; (2) background (Function 1, shifted Chebyschev); (3) scale factors; (4) unit-cell dimensions; (5) March-Dollase preferred orientation parameters; (6) terms *LX* and *LY* in the profile function (Function 2, pseudo-Voigt); (7) atomic coordinates; (8) site occupancies of Na and Ca at the *M*(4) and of Na at the *A* site, and (9) isotropic displacement parameters (U_{iso}) if they could be stably refined. Site occupancies at the *T*(1) and *M*(2) sites were assumed to be fully occupied by Si and Al, respectively, because of the similarities in the scattering factors of Si, Al, and Mg. For short scans, refinements only involved the zero point, background, scale factors, March-Dollase preferred orientation, and cell dimensions, where the cell dimensions of the amphiboles are used to gauge the extent of compositional re-equilibration, as discussed below..

Electron microprobe (EMP) analysis was accomplished on a JEOL 8900 Superprobe. Samples were mounted in epoxy, polished with diamond grit in steps down to 0.5 μm, carbon coated, and analyzed under the conditions of 15 kV and 10 nA. The standards used were: diopside for Ca, albite for Na, and the pure oxides for Mg, Al, and Si.

We measured Fourier transform infrared spectra (FTIR) as mid-infrared spectra (MIR) and far-infrared spectra (FIR) at two different institutions. For the MIR spectra two sets of samples were prepared, one by embedding the sample in KBr pellets using a sample/KBr ratio of 0.7mg/200mg for measurements in the lattice-vibration range (350–2000 cm^{-1}), the

other using a sample/KBr ratio of 3mg/200mg for measurements in the OH-stretching region (2000–4000 cm^{-1}). All pellets were prepared by compression in an evacuated die. MIR spectra were recorded in transmission mode with a Bruker Equinox 55 spectrometer at Binghamton University scanned 64 times at a resolution of 2.0 cm^{-1} under flowing nitrogen. The FIR spectra were obtained at Kyushu University, Japan, with a JASCO FTIR-620 spectrometer using either a Hg-lamp with 12 μm Mylar beam splitter or a globar source with 5μm Mylar beam splitter. Two sets of spectra were recorded: (1) a small sample concentration of 0.8–1.1 mg and (2) a large sample concentration of 1.9–2.6 mg, both embedded in about 80 mg polyethylene discs 10 mm in diameter. These two concentrations were used in an attempt to improve the signal-to-noise ratio in different portions of the spectra. Samples were scanned 512 times at a resolution of 2 cm^{-1} in the range of 650–50 cm^{-1}.

RESULTS

Amphibole yield

We synthesized individual amphiboles along the Hb–Gl join at conditions ranging from 760°C/2.5GPa (Gl-rich) to 860°C/1.3GPa (Hb-rich) for 72–216 hours. In general, excellent amphibole yields (92% –100%) were obtained. From Table 2, it is obvious that the Hb-rich amphiboles have a better yield than the Gl-rich counterparts, including even pure yields of amphibole, such as MgHG-(R)4-2, MgHG-(R)8-2 (Fig. 1A) and MgHG-11. Talc is the most common additional phase, though some of the extra phases can be removed during retreatment by increasing the reaction temperature. However, increasing the temperature may produce an amorphous phase, as seen for example by an elevated background in the XRD pattern of MgHG-(R)7-2.2 (Fig. 1b). This amorphous phase does not always coexist with talc, and in fact only appeared in MgHG-(R)7-2.2. It is not clear if it is a quenched silicate

melt or a solute that percipitates from the ambient fluid upon quench. Besides talc and this amorphous material, quartz and smectite also occur in the run products, but typically have an abundance below 10 wt %. Rarely pyroxene crystallized during the synthesis but generally could be eliminated with retreatment.

Amphibole compositions and textures

Amphibole compositions are listed in Table 3 and shown in Figures 2a and 2b. Projection of the synthesized amphibole compositions (open circles) from SiO_2 and H_2O into the Na_2O-CaO-MgO-Al_2O_3 tetrahedron in Figure 2a shows that the samples lie close to the intended join "A"–Gl (solid circles) and are closely modeled by the amphibole sub-tetrahedron Hb–Gl –Cm–Kt, where Cm is cummingtonite [$^{A}\square^{B}Mg_2{}^{C}Mg_5{}^{T}Si_8O_{22}(OH)_2$] and Kt is katophorite [$^{A}Na^{B}(NaCa)^{C}(Mg_4Al)^{T}(AlSi_7)O_{22}(OH)_2$]. The latter component is included because deviation of sodium- and sodium-calcium-amphiboles toward enrichment in the katophorite component was noted in earlier studies (Graham et al. 1989; Pawley 1992; Jenkins et al. 2013). Compositional departures from the intended join are more apparent in Figure 2b, where the synthesized amphibole compositions (open circles) are projected from cummingtonite, quartz, and water onto the Gl–Tr–Ts ternary plane. This diagram demonstrates that small deviations from the intended join exist indicating some depletion in the Ts component near the middle of the join, but not significantly outside of the range of uncertainty for any given point as indicated by the representative error bars on Figure 2b. Overall, the agreement between the nominal and observed amphibole compositions is quite close as expected from the high synthesis yields.

Figure 3 presents representative back-scattered electron (BSE) images of the amphiboles synthesized in this study. Figure 3a is from a sample that lies mid-way along this join (Gl_{50}). Crystals are bigger and more easily identified than at the Gl-rich end (Fig. 3b), where the grains occur as very fine-grained aggregates. Near the Hb-rich end of the join (Figs. 3c,d) the

amphibole grains are distinctly larger.

Unit-cell dimensions

Table 4 lists unit-cell dimensions for individual synthetic amphiboles determined from Rietveld refinements of the powder XRD patterns. Table 4 also includes selected whole-pattern agreement indices. Unit-cell dimensions are plotted in Figure 4a (open circles) as a function of Ca content (apfu). The curve fitted to the volume data is a polynomial regression, given in the figure, and includes the end-member volume for glaucophane (solid circle, 863 $Å^3$) from the study of Jenkins and Corona (2006b). In order to gauge the effect of non-binary components on unit-cell volumes, the compositions of the amphiboles were recast into the components Gl, Hb, Cm, and Kt, which are given in Table 5, using the site-occupancy relations listed in the footnote to the table. Although this set of component is not unique, these components were chosen because they closely model the amphiboles formed in this study (Fig. 2a) and because the volumes of the components Cm and Kt are relatively well known, as noted below. Volumes were corrected back to the Hb–Gl join assuming a linear change in volume over relatively small changes in composition according to the relationship:

$$V_{corr} = [V_{obs} - (X_{Cm} \cdot V_{Cm} + X_{Kt} \cdot V_{Kt})]/(X_{Gl} + X_{Hb}) \quad (1)$$

where V_{obs} is the observed volume, X_i is the mole fraction of component i, and V_i is the volume of pure component i. The unit-cell volumes adopted for this study are V_{Cm} = 874.4 $Å^3$ (extrapolated from heated - *C*2/*m* - samples in the cummingtonite–grunerite join; Hirschmann et al. 1994) and V_{Kt} = 893.1 $Å^3$ (Jenkins et al. 2013).

Table 5 lists the calculated values of V_{corr} using Equation (1) and the mole fraction of the Hb component corrected for Cm and Kt, called Hb'. The corrected volumes are plotted against Hb' in Figure 4b. The solid curve is a polynomial (given in the figure) fit to the data but weighted by the inverse of the error in V_{corr} because of the large range (factor of 25) in the uncertainties of the corrected volumes. The dashed curve in Figure 4b is the polynomial fit to

the original volume data from Figure 4a and is reported for comparison. As seen in Figure 4b, the volume correction causes only a modest shift in the volume-composition relationships.

Two observations can be drawn from the relations given in Figure 4. First, the volume of end-member magnesio-hornblende (Hb' = 1.0) calculated from the polynomial given in Figure 4b gives a volume of 900.5 ± 3.0 $Å^3$. This is in excellent agreement with the volume of end-member magnesio-hornblende derived from cell-dimension equations reported by Najorka and Gottschalk (2003, 899 $Å^3$, solid triangle) based on their study of amphiboles formed along the tremolite–tschermakite join, but larger than the volume given by the equations in Hawthorne and Oberti (2007, 892 $Å^3$, solid square) based on multiple regression analysis of the extensive IGG-CNR-PV amphibole database. It appears that the unit-cell volume of magnesio-hornblende based on experimental studies of chemically simplified systems are converging to a value of about 900 $Å^3$; the reason for the discrepancy with the value derived from the IGG-CNR-PV amphibole database is unknown at this time. Second, the volume data, whether corrected or not for non-binary components, show a clear positive deviation from an ideal (straight line) trend. This indicates an excess volume of mixing between the Hb and Gl components and is consistent with a positive enthalpy of mixing along this join (e.g., Davies and Navrotsky 1983) and the potential presence of a miscibility gap.

Glaucophane and amphibole "A" re-equilibration experiments

A second set of experiments were done to locate the miscibility gap along this join, or at least to provide constraints on the temperature of the critical point. Synthetic amphibole "A" and glaucophane were mixed in a molar ratio of 1:1 (MgHG-mixture) and treated at the conditions listed in Table 6 to determine if they would undergo homogenization to either a single amphibole or to a mixture of two coexisting amphiboles. Using end-member

compositions in these experiments means that incomplete re-equilibration would define only the maximum extent of the miscibility gap because the reaction rate becomes slower near the equilibrium phase boundary. The run products of these treatments are mainly one or two amphiboles with minor talc, smectite, and/or quartz (Table 6). We made no attempt to try and define the minimum width of the miscibility gap by exsolution of a single-phase amphibole into two amphiboles owing to the low temperatures involved (< 700°C) and the limited success of this approach for the closely-related tremolite-glaucophane join reported by Jenkins et al. (2014).

Documenting changes in amphibole composition by electron microprobe analysis for these fine-grained amphiboles (Fig. 3) is difficult and gave highly scattered results for the tremolite-glaucophane join (Jenkins et al. 2014). Instead, we have employed the volume-composition relationship given in Figure 4a for amphiboles formed in this study, to determine their compositions. Although an indirect analytical method, it has the distinct advantage of providing the average composition of a large number of grains because the X-ray beam typically covers at least 50% of the sample area in the angular range (20–40 °2Θ) of maximum peak intensities. The volumes of single-phase or coexisitng amphiboles were measured by XRD analysis, refined with the program GSAS, and are listed in Table 7. We note here that the Rietveld full-pattern method is well suited for dealing with mixtures of phases of similar structure (e.g., feldspars) as discussed by Bish and Post (1993), so long as the reflections are sufficiently well resolved. Treatments at 800 and 750 °C readily re-equilibrated to a single, homogeneous amphibole; however, at 700 °C and lower the reaction rate was slower. Therefore, time-series experiments were implemented to provide some sense of the rate of compositional change. Figure 5 shows the change in amphibole composition with time for samples treated at 600, 650, and 700 °C. At 600 and 650 °C (Figs. 5a and 5b) we detected no statistically significant change in amphibole compositions and

relative peak heights after 11 and 14 days, respectively, and further treatments were halted. However, at 700 °C (Fig. 5c) there was a noticeable change in compositions of the amphiboles after the first 10 days and treatments were continued until the two amphiboles gradually homogenized to a single amphibole after about 20 days. The XRD powder patterns for the 700 °C series are shown in Figure 6 (MgHG-M_2-series from Table 7), where some of the readily resolved peaks of glaucophane are indicated by arrows labeled with their Miller indices. The marked peaks show a tendency to either decrease in intensity or combine with the hornblende peaks and then gradually become sharper going from the bottom pattern (starting mixture) to the top (final treatment).

The results of the amphibole re-equilibration experiments are shown on the temperature-composition diagram in Figure 7. The small solid dots indicate the starting composition of the amphiboles, also determined using the volume-composition equation of Figure 4a, whereas the open circles and squares indicate the compositions of re-equilibrated Gl-rich and Hb-rich amphiboles, respectively. The arrows show the sense of composition change. Note that the Gl-rich amphiboles at 600 and 650 °C show either very little change or even a small decrease in their Ca contents. Such minor Ca variations are probably within the analytical precision of this method; however, this is the strongest evidence that the Ca-poor side of the miscibility gap has a fairly steep limb whereas the Ca-rich side slopes more gently. Such behavior is observed in other joins where the steeper limb occurs near the end-member with the smaller cation as seen, for example, for the joins enstatite–dopside (Lindsley and Dixon 1976), halite– sylvite (Walker et al. 2005), and albite–orthoclase (Benisek et al. 2014). The miscibility gap shown in Figure 7 was calculated as discussed below.

Autocorrelation analysis of FTIR spectra

Spectra in the mid-infrared range (MIR) were recorded at 350–4000 cm^{-1} and lattice-vibration region, which is considered to be more sensitive to inter-atomic strain, is presented in Figure

8. We consider interference from non-amphibole phases in the lattice vibration region to be negligible because of the high amphibole yields in this study (Table 2). In the region 800–700 cm^{-1}, the relatively sharp and well-defined absorption bands observed for the end-member spectra become broader bands for the intermediate compositions, consistent with the development of increased strain at the more highly-mixed intermediate compositions (e.g., Carpenter 2002). In addition, a gradual shift in the band positions above 600 cm^{-1} to higher wavenumbers occurs with increasing Gl content (from bottom to top) indicating an increase in vibration frequencies with reduction in unit-cell volume. Far-infrared spectra (FIR) in the range of 100-350 cm^{-1} shown in Figure 9 exhibit a similar band broadening for intermediate compositions but no consistent shift in band frequencies with change in composition.

Autocorrelation analysis has been applied to four wavenumber ranges, namely, (i) 162–224 cm^{-1} (= 200 cm^{-1}), (ii) 328–407 cm^{-1} (= 360 cm^{-1}), (iii) 410–610 cm^{-1} (= 500 cm^{-1}), and (iv) 620–1300 cm^{-1} (= 800 cm^{-1}). The observed changes in band widths, expressed by the parameter $\Delta Corr$ (cm^{-1}), are plotted as a function of composition in Figure 10. Only the results for the 200 and 800 cm^{-1} ranges yielded systematic variations in $\Delta Corr$, whereas the 360 and 500 cm^{-1} ranges yielded highly scattered values. Figure 11 shows the same data but expressed as $\delta\Delta Corr$, namely the difference between $\Delta Corr$ and the straight baseline between the end members of the join as illustrated in Figure 10d. The $\delta\Delta Corr$, or relative band-width changes, have been correlated with enthalpy of mixing (Boffa-Ballaran and Carpenter 2003; Etzel and Benisek 2008). Even if absolute values of the enthalpy of mixing (ΔH^{Mix}) can not yet be reliably derived from the autocorrelation data, it was argued by Jenkins et al. (2014) that the positive deviation from ideal mixing and the sense of asymmetry in the mixing along a compositional join should be revealed by the autocorrelation results. Results from the 360 and 500 cm^{-1} ranges are too scattered to be useful; however, a two-parameter asymmetric Margules formulation (e.g., Davies and Navrotsky 1983) was used to model the $\delta\Delta Corr_{200}$

and $\delta\Delta Corr_{800}$ data in Figures 11a and 11d. The excess Gibbs free energy of mixing can be approximated by the enthalpy of mixing and therefore $\delta\Delta Corr$ as follows:

$$\Delta G^{\text{Excess}} \approx \Delta H^{\text{Mix}} \propto \delta\Delta Corr = (W_{\text{Gl}}X_{\text{Hb}} + W_{\text{Hb}}X_{\text{Gl}})X_{\text{Gl}}X_{\text{Hb}} \quad (2)$$

where X_i is the mole fraction of end-member i and W_i is the corresponding interaction parameter. Equation (2) was used to fit the $\delta\Delta Corr_{200}$ and $\delta\Delta Corr_{800}$ data with the resulting interaction parameters, in units of wavenumbers, indicated on Figures 11a and 11d, respectively. Although there is clearly a positive deviation from ideal mixing of the end-members, the rather surprising result is that the sense of asymmetry in the mixing energetics is the opposite of what is expected, with the data skewed towards the larger-volume rather than the smaller-volume Gl-rich portion of the join. A similar situation was encountered for the Ca-Tschermak–diopside join by Etzel and Benisek (2008), where the skew of the $\delta\Delta Corr$ data was opposite to the calorimetrically measured ΔH^{Mix}. A resolution to these apparently contradictory results between the dissolution experiments and autocorrelation analysis will be offered below.

Short-range ordering

Because OH-stretching bands in amphibole are sensitive to the local atomic environment, important additional information about the octahedral, tetrahedral, and A-site cation occupancy near the OH group can be determined (e.g., Della Ventura et al. 1999; Hawthorne et al. 2000). Therefore, a second set of MIR spectra were measured with an increased sample/KBr ratio of 3/200 mg to enhance the intensity in the OH-stretching region. Essentially all of the spectra had broad bands centered at about 3500 cm^{-1} attributed to moisture absorbed by the sample. Spectra that could be adequately modeled with symmetric pseudo-Voigt profiles and from which band positions and relative intensities were extracted are listed in Table 8. Several spectra are shown in Figure 12, where the dots are the observed and the solid curve the modeled spectrum.

401 The configuration notation used throughout the following discussion was introduced by
402 Della Ventura et al. (1999) and Hawthorne et al. (2000). End-member glaucophane (MgHG-
403 10-2.2, Fig. 12), with essentially no ^{T}Al and no ^{A}Na (Table 3), has only one readily
404 identifiable asymmetric band, similar to the Gl-rich spectra reported earlier by Palin et al.
405 (2003), Jenkins and Corona (2006a). We chose to model this with two bands, the dominant
406 band (B) at 3664 cm^{-1} and a smaller shoulder band (B') at 3674 cm^{-1}. The B band occurs in all
407 of the samples in the range 3664–3674 cm^{-1} and is assigned to the MgMgMg-□-SiSi
408 configuration for the *M*(1)*M*(1)*M*(3)-*A*-*T*(1)*T*(1) sites (e.g., Della Ventura et al. 2003). This
409 band shifts from 3670 cm^{-1} for Hb-rich to 3664 cm^{-1} for Gl-rich amphiboles, which is
410 consistent with the small shift to lower frequencies with substitution of Na at the *M*(4) and Al
411 at the *M*(2) sites, both fairly distant from the O(3) site, in glaucophane as observed by Jenkins
412 et al. (2013) and as observed for *M*(4) site substitutions in richteritic amphiboles by Iezzi et
413 al. (2010). The shoulder B' band in end-member glaucophane is also attributed to the
414 MgMgMg-□-SiSi configuration, but having Mg rather than Na at the neighboring *M*(4) sites,
415 as proposed by Jenkins et al. (2013) and supported by the presence of ^{B}Mg in this sample
416 (Table 3).
417 The remaining spectral features can be divided into two regions using band B as the
418 center: one having lower frequencies (e.g., bands A and A') corresponding to substitutions at
419 the octahedral and tetrahedral sites in A-site-vacant local configurations, and one at higher
420 frequencies (e.g., bands C and D) corresponding to the region of A-site-filled local
421 configurations. At lower frequencies, band A occurs in the range of 3651–3658 cm^{-1} for the
422 Hb-rich samples. Interference from adjacent water absorption bands makes determination of
423 the A band's relative intensity difficult which may result in spuriously high values listed in
424 Table 8. This band is assigned to the MgMgMg-□-SiAl configuration because of an overall
425 increase in its intensity with increasing Hb component (Table 8) and because it has a

426 frequency shift consistent with substitution of Al at the *T*(1) site (Hawthorne et al. 2000).
427 Substitution of Al at the more distant *M*(2) site produces only a small inductive shift in the
428 OH-vibration, but substitution of Al at the *M*(1) or *M*(3), typical of synthetic and more
429 disordered amphiboles, should produce a noticeable shift to lower frequencies. The fairly
430 low intensity band A' at 3644–3646 cm^{-1} for samples MgHG-(R)9, MgHG-(R)5-2.2, and
431 MgHG-3.2 is assigned to the MgMgAl-□-SiSi configuration (Hawthorne et al. 2000; Della
432 Ventura et al. 2003) because of the large frequency shift. The occurrence of this weak band
433 in amphiboles with high ^{C}Al content (Table 8) suggests minor Al at the M(3) site (Oberti et
434 al. 1995). At higher frequencies, band C at 3681–3700 cm^{-1} and band D at 3709–3742 cm^{-1}
435 appear in samples containing appreciable ^{A}Na (Table 8); accordingly, these bands are
436 assigned to the MgMgAl-Na-SiAl and MgMgMg-Na-SiSi configurations, respectively,
437 proposed by Della Ventura et al. (1999, 2003). From these observations, we conclude that
438 independent evidence exists for Na on the A site, association of Na with both Si as well as Al
439 at the *T*(1) sites, and the presence of some Al at the *M*(3) in addition to the *M*(2) sites,
440 although the degree of disorder is unknown at present.
441

442 ## DISCUSSION

443 The development of composition-activity relations for chemically complex amphiboles
444 has been a goal for decades, especially involving cation mixing derived from coexisting
445 amphiboles (e.g., Powell 1975). Because magnesio-hornblende is an intermediate
446 composition between the end-members tremolite and tschermakite, one can use constraints on
447 the location of the miscibility gap between magnesio-hornblende and glaucophane provided
448 in this study to refine the mixing properties of amphibole in the ternary system tremolite-
449 glaucophane-tschermakite involving mixing of Ca and Na at the B, Al and Mg at the C, and
450 Al and Si at the T crystallographic sites. Holland and Powell (2003) developed a means of

451 modeling non-symmetric interactions for chemically complex phases, such as amphiboles,
452 using a method referred to as asymmetric formalism (ASF). As discussed in detail by Dale et
453 al. (2005), asymmetric mixing among the three components Gl, Tr, and Ts dealt with in this
454 study requires six variables: three macroscopic interaction parameters ($W_{\mathrm{Gl,Tr}}$, $W_{\mathrm{Gl,Ts}}$, and
455 $W_{\mathrm{Tr,Ts}}$) and three size parameters (α_{Gl}, α_{Tr}, and α_{Ts}). Activities of individual components
456 can be calculated as the product of the ideal activity ($a_{\mathrm{i}}^{\mathrm{ideal}}$) and the corresponding activity
457 coefficient (γ_{i}). Ideal activities for Gl and Tr, the two components used here to model the
458 miscibility gaps shown in the system Na_2O-CaO-MgO-Al_2O_3-SiO_2-H_2O, are:

459 $$a_{\mathrm{Gl}}^{ideal} = X_{\square}^{\mathrm{A}}\left[X_{\mathrm{Na}}^{\mathrm{M4}}\right]^2\left[X_{\mathrm{Al}}^{\mathrm{M2}}\right]^2\left[X_{\mathrm{Si}}^{\mathrm{T1}}\right] \quad (3a)$$

460 $$a_{\mathrm{Tr}}^{ideal} = X_{\square}^{\mathrm{A}}\left[X_{\mathrm{Ca}}^{\mathrm{M4}}\right]^2\left[X_{\mathrm{Mg}}^{\mathrm{M2}}\right]^2\left[X_{\mathrm{Si}}^{\mathrm{T1}}\right] \quad (3b)$$

461 where X_i^j is the mole fraction of cation *i* on site *j,* the *M*(1) and *M*(3) sites are fully occupied
462 by Mg, and □ is a vacancy. Note that the mole fraction on the tetrahedral [(*T*)1] site is only
463 raised to the first (rather than the fourth) power, as suggested by Dale et al. (2005), to
464 minimize the magnitude of the activity coefficient for this component. The corresponding
465 activity coefficient for the Gl and Tr components are then calculated for the ternary
466 amphibole system tremolite–glaucophane–tschermakite as:

467 $$\begin{aligned} RT\ln(\gamma_{\mathrm{Gl}}) = {} & (1-\phi_{\mathrm{Gl}})(\phi_{\mathrm{Tr}})W_{\mathrm{Gl,Tr}}\left[\frac{2\alpha_{\mathrm{Gl}}}{(\alpha_{\mathrm{Gl}}+\alpha_{\mathrm{Tr}})}\right] \\ & + (1-\phi_{\mathrm{Gl}})(\phi_{\mathrm{Ts}})W_{\mathrm{Gl,Ts}}\left[\frac{2\alpha_{\mathrm{Gl}}}{(\alpha_{\mathrm{Gl}}+\alpha_{\mathrm{Ts}})}\right] \\ & - (\phi_{\mathrm{Ts}})(\phi_{\mathrm{Tr}})W_{\mathrm{Tr,Ts}}\left[\frac{2\alpha_{\mathrm{Gl}}}{(\alpha_{\mathrm{Tr}}+\alpha_{\mathrm{Ts}})}\right] \end{aligned} \quad (4a)$$

$$RT\ln(\gamma_{\mathrm{Tr}}) = (1-\phi_{\mathrm{Tr}})(\phi_{\mathrm{Gl}})W_{\mathrm{Gl,Tr}}\left[\frac{2\alpha_{\mathrm{Tr}}}{(\alpha_{\mathrm{Gl}}+\alpha_{\mathrm{Tr}})}\right] + (1-\phi_{\mathrm{Tr}})(\phi_{\mathrm{Ts}})W_{\mathrm{Tr,Ts}}\left[\frac{2\alpha_{\mathrm{Tr}}}{(\alpha_{\mathrm{Tr}}+\alpha_{\mathrm{Ts}})}\right] - (\phi_{\mathrm{Ts}})(\phi_{\mathrm{Gl}})W_{\mathrm{Gl,Ts}}\left[\frac{2\alpha_{\mathrm{Tr}}}{(\alpha_{\mathrm{Gl}}+\alpha_{\mathrm{Ts}})}\right] \quad (4b)$$

where $\phi_i = (\alpha_i p_i)/(\alpha_{\mathrm{Gl}}p_{\mathrm{Gl}} + \alpha_{\mathrm{Tr}}p_{\mathrm{Tr}} + \alpha_{\mathrm{Ts}}p_{\mathrm{Ts}})$ and p_i is the mole fraction of component i. The activities of the Gl and Tr components are therefore the product of the ideal activity and activity coefficient, namely:

$$a_{\mathrm{GL}} = a_{\mathrm{Gl}}^{ideal} \cdot \gamma_{\mathrm{Gl}} \quad (5a)$$

$$a_{\mathrm{Tr}} = a_{\mathrm{Tr}}^{ideal} \cdot \gamma_{\mathrm{Tr}} \quad (5b)$$

and the condition for equilibrium between coexisting Gl-rich and Tr-rich amphiboles can be expressed as:

$$a_{\mathrm{Gl}}^{\mathrm{glaucophane}} = a_{\mathrm{Gl}}^{\mathrm{tremolite}}$$
$$a_{\mathrm{Tr}}^{\mathrm{glaucophane}} = a_{\mathrm{Tr}}^{\mathrm{tremolite}} \quad (6)$$

Values for the six parameters of interest were reported earlier by Diener and Powell (2012) based on natural two-amphibole assemblages; however, the experimental data given in this study on compositionally simpler amphiboles and with known values of P and T provide strong constraints on some of these parameters by avoiding the influence of other elements. Because only the relative values of α_i are important, it is customary to set one of the size parameters to unity, which is normally α_{Tr} (e.g., Diener et al. 2007). The values of $W_{\mathrm{Gl,Tr}}$ and α_{Gl} were adopted from the study of Jenkins et al. (2014) as being 70 kJ and 0.52, respectively. The miscibility gap investigated in this study was considered to provide better constraints on $W_{\mathrm{Gl,Ts}}$ than on $W_{\mathrm{Tr,Ts}}$ because of the proximity of the miscibility gap to glaucophane (Figs. 7, 13); therefore, the parameters $W_{\mathrm{Gl,Ts}}$ and α_{Ts} were allowed to vary whereas the value of $W_{\mathrm{Tr,Ts}}$ was taken from Diener and Powell (2012).

Values for the best-fit interaction and size parameters are listed in Table 9, with a set of isotherms through the ternary miscibility gap calculated using these parameters shown in Figure 13a; also shown are the compositions of amphiboles that limit the locations of these miscibility gaps. Data points along the tremolite-glaucophane join are from Jenkins et al. (2014) whereas data along the amphibole-"A"–glaucophane join are from this study. The points on the Tr- and Hb-rich side of the miscibility gaps lie noticeably off the gap because, as indicated above, these compositions probably indicate the absolute maximum width of the two-phase field at a given temperature because of sluggish re-equilibration kinetics. On the Gl-rich side of the miscibility gap the agreement is much better, with the highest-temperature data (700°C) considered to have the closest approach to equilibrium and the corresponding closest fit. In addition to the limiting amphibole compositions, the cation mixing properties are strongly constrained by having the critical point lie below 700°C for compositions along the amphibole-"A"–glaucophane join (Fig. 7). The shape of the solvus shown in Figure 7 can now be recognized as the intersection of the isotherms of the ternary miscibility gap with the "A"–Gl join. A 4th-order polynomial, namely $T(°C) = 370.70 + 1535.32(Ca) - 2558.81(Ca^2) + 1653.95(Ca^3) - 411.53(Ca^4)$ where Ca is in atoms per formula unit (apfu), was used to model the solvus. This polynomial is provided only for the purpose of graphical representation and has no physical meaning.

Figure 13b shows a representative isothermal section with tie-lines connecting coexisting amphibole compositions. Note that the orientation of these tie-lines rotates toward the Ts corner as they converge at the critical-point composition (solid circle) on the miscibility gap. This behavior exists for any given isothermal section, and the critical points at any given temperature project as the grey curve shown on the figure. The compositional join "A"-Gl crosses the critical curve at a Ca content of 1.10 apfu. This composition corresponds to the maximum in the excess Gibbs free energy (G^{excess}) shown in Figure 14, where G^{excess} is

513 calculated in ASF theory (Holland and Powell 2003) as:

514 $G^{excess} = \square_{Gl}\,\square_{Tr}B_{GlTr} + \square_{Gl}\,\square_{Ts}B_{GlTs} + \square_{Tr}\,\square_{Ts}B_{TrTs}$ (7)

515 where the values of $\square_i$ are the same as defined previously and B_{ij} is calculated as B_{ij} =

516 $2\alpha_k p_k/(\alpha_i + \alpha_j)$ with k ≠ i, j.

517 We can now offer some explanation for the contradiction between the sense of
518 miscibility-gap asymmetry indicated by the autocorrelation results shown in Figure 11 and its
519 shape in Figure 7. Realizing that the join investigated in this study is a section through the
520 ternary system tremolite–glaucophane–tschermakite, the tie-lines join amphiboles whose
521 compositions lie outside of the bounds of this pseudo-binary section, not within the section,
522 and converge to critical points that are relatively Ca-rich. For the two frequency ranges that
523 yielded a clear autocorrelation signal, namely the 162–224 cm^{-1} ("200" cm^{-1}) and 620–1300
524 cm^{-1} ("800" cm^{-1}) ranges, the maximum values of $\delta\Delta Corr$ are in the Ca ranges of 1.15–1.4
525 and 0.9–1.38 apfu, respectively, which are relatively close to the maximum of 1.10 apfu in
526 the G^{excess} curve of Figure 14. We stress that placement of the isotherms in Figure 13a was
527 based solely on the composition-temperature constraints (Figs. 5, 7) on the location of the
528 miscibility gap along the tremolite–glaucophane and magnesio-hornblende–glaucophane
529 joins and was done independently of the autocorrelation results in Figure 11.
530

531 ## IMPLICATIONS

532 The magnesio-hornblende–glaucophane join studied here along with the thermodynamic
533 modeling of the two-amphibole region in the tremolite–glaucophane–tschermakite ternary
534 system provide important insights into the compositional variations observed for sodium- and
535 calcium-sodium-amphiboles in nature. Brown (1977) compiled amphibole compositions
536 from a variety of metamorphic terranes where the amphibole compositions were buffered by
537 coexisting albite, chlorite, and iron oxide. The resultant "geo-experimental" diagram (cf.,

Newton 2011), reproduced as Figure 15a here, shows systematic variations in the Na content of the *M*(4) site with Al at the *T*(1) site, so long as the amphiboles occur in equilibrium with the buffering minerals. These variations were considered to be controlled primarily by pressure. Although Brown (1977) noted that a miscibility gap might exist between calcium- and sodium-amphiboles at high *P*, he proposed that there was complete miscibility at the greenschist or lower-pressure portion of the blueschist facies. Figure 15a from Brown (1977), being both an elegant and simple use of calcium-amphibole chemical variations to deduce *P*, has been cited often since its publication, with an average yearly citation of ~200 (Web of Science 2014).

The ternary system tremolite–glaucophane–tschermakite comprises essentially all of the amphibole compositions shown in Figure 15a, so that the results from this study should have some relevance to this diagram. Figure 15b has the isotherms from Figure 13a superimposed on it. The amphibole compositions from the Otago, Shuksan, and Sanbagawa terranes agree closely with the isotherms at 500–550 °C. Although Brown (1977) discounted the role of amphibole immiscibility in this diagram, the striking agreement between the amphibole compositions observed in nature and the lower-temperature portion of the miscibility gap determined in this study suggests immiscibility may be more important than pressure. Since the study of Brown (1977), evidence has been presented for coexisting sodium- and calcium-amphiboles in low-grade metabasaltic rocks from various blueschist-facies terranes (e.g., Ernst 1979). Further improvements in quantifying the conditions under which calcium-rich and sodium-rich amphiboles form in the presence of the buffering mineral assemblage can be obtained by extending the mixing properties of amphiboles to include ferrous- and ferric-iron components. Preliminary results of amphibole compositions coexisting with chlorite, plagioclase, and epidote in a model mid-ocean-ridge basalt bulk composition using the parameters derived from this study, with the parameters for other amphibole components

563 (e.g., Diener and Powell 2012), were presented by Jenkins and Lei (2013) and will be the
564 subject of a more detailed publication.
565

566 ## ACKNOWLEDGEMENTS

567 Financial support for this study was provided by NSF grant EAR-0947175 to DMJ. We
568 thank David Collins for his help with the electron microprobe analyses. The manuscript was
569 greatly improved by the thorough reviews of W. G. Ernst and G. Iezzi.
570

571 ## REFERENCES CITED
572
573 Atkinson, A.J., Carpenter, M.A., and Salje, E.K.H. (1999) Hard-mode infrared spectroscopy
574 of plagioclase feldspars. European Journal of Mineralogy, 11, 7–21.
575 Basora, A.M., Jenkins, D.M., and Bish, D.L. (2012) The lower-pressure stability of
576 glaucophane in the presence of paragonite and quartz in the system Na_2O-MgO-Al_2O_3-
577 SiO_2-H_2O. American Mineralogist, 97, 713-726.
578 Benisek, A., Dachs, E., and Kroll, H. (2014) Thermochemistry of the alkali feldspars:
579 Calorimetric study of the entropy relations in the low albite—low microcline series.
580 American Mineralogist, 99, 76-83.
581 Bish, D.L., and Post, J.E. (1993) Quantitative mineralogical analysis using the Rietveld full-
582 pattern fitting method. American Mineralogist, 78, 932-940.
583 Boffa Ballaran, T. and Carpenter, M.A. (2003) Line broadening and enthalpy: some
584 empirical calibrations of solid solution behaviour from IR spectra. Phase Transitions, 76,
585 137-154.
586 Boffa Ballaran, T., Carpenter, M.A., Domeneghetti, M.C., Salje, E.K.H., and Tazzoli, V.
587 (1998) Structural mechanism of solid solution and cation ordering in augite–jadeite
588 pyroxenes II: a microscopic perspective. American Mineralogist, 83, 419–433.

589 Boffa Ballaran, T., Carpenter, M.A., Geiger, C.A., and Koziol, A.M. (1999) Local structural
590 heterogeneity in garnet solid solutions. Physic and Chemistry of Minerals, 26, 554–569.
591 Boffa Ballaran, T., Carpenter, M.A., and Domeneghetti, M.C. (2001) Phase transition and
592 mixing behaviour of the cummingtonitengtonitein solid solution. Physics and Chemistry
593 of Minerals, 28, 87try o
594 Bozhilov, K.N., Brownstein, D., and Jenkins, D.M. (2007) Biopyribole evolution during
595 tremolite synthesis from dolomite and quartz in CO_2-H_2O fluid. American Mineralogist,
596 92, 898-908.
597 Brown, E.H. (1977) The crossite content of Ca-amphibole as a guide to pressure of
598 metamorphism. Journal of Petrology, 18, 53-72.
599 Cao, R.L., Ross, C., and Ernst, W.G. (1986) Experimental studies to 10 kb of the bulk
600 composition tremolite$_{50}$-tschermakite$_{50}$ + excess H_2O. Contributions to Mineralogy and
601 Petrology, 93, 160-167.
602 Carpenter, M.A. (2002) Microscopic strain, macroscopic strain and the thermodynamics of
603 phase transitions in minerals. In, C.M. Gramaccioli (ed.) Energy Modelling in Minerals,
604 European Mineralogical Union Notes in Mineralogy, 4, 311-346.
605 Carpenter, M.A. and Boffa Ballaran, T. (2001) The influence of elastic strain heterogeneities
606 in silicate solid solutions. In, C.A. Geiger (ed.) Solid Solutions in Silicate and Oxide
607 Systems, European Mineralogical Union notes in Mineralogy, 3, 155–178.
608 Cho, M. and Ernst, W.G. (1991) An experimental determination of calcic amphibole solid
609 solution along the join tremolite-tschermakite. American Mineralogist, 76, 985–1001.
610 Corona, J.C. and Jenkins, D.M. (2007) An experimental investigation of the reaction:
611 glaucophane + 2 quartz = 2 albite + talc. European Journal of Mineralogy, 19, 147-158.
612 Corona, J.C., Jenkins, D.M., and Holland, T.J.B. (2013) Constraints on the upper pressure
613 stability of blueschist facies metamorphism along the reaction: glaucophane = talc + 2

614 jadeite in the Na_2O-MgO-Al_2O_3-SiO_2-H_2O system. American Journal of Science, 313,
615 967-995.
616 Davies, P.K., and Navrotsky, A. (1983) Quantitative correlations of devations from ideality in
617 binary and pseudobinary solid solutions. Journal of Solid State Chemistry, 46, 1-22.
618 Dale, J., Powell, R., White, R.W., Elmer, F.L., and Holland, T.J.B. (2005) A thermodynamic
619 model for Ca-Na clinoamphiboles in Na_2O-CaO-FeO-MgO-Al_2O_3-SiO_2-H_2O-O for
620 petrological calculations. Journal of Metamorphic Geology, 23, 771-791.
621 Della Ventura, G., Hawthorne, F.C., Robert, J.-L., Delbove, F., Welch, M.D., and Raudsepp,
622 M. (1999) Short-range order of cations in synthetic amphiboles along the richterite-
623 pargasite join. European Journal of Mineralogy, 11, 79-94.
624 Della Ventura, G. Hawthorne, F.C., Robert, J.-L., and Iezzi, G. (2003) Synthesis and infrared
625 spectroscopy of amphiboles along the tremolite-pargasite join. European Journal of
626 Mineralogy, 15, 341-347.
627 Diener, J.F.A. and Powell, R. (2012) Revised activity-composition models for clinopyroxene
628 and amphibole. Journal of Metamorphic Geology, 30, 131-142.
629 Diener, J.F.A., Powell, R., White, R. W., and Holland, T.J.B. (2007) A new thermodynamic
630 model for clino- orthoamphiboles in the system Na_2O-CaO-FeO-MgO-Al_2O_3-SiO_2-H_2O-
631 O. Journal of Metamorphic Geology, 25, 631-656.
632 Evans, B.W., Ghiorso, M.S., and Kuehner, S.K. (2000) Thermodynamic properties of
633 tremolite: A correction and some comments. American Mineralogist, 85,466-472.
634 Ernst, W.G. (1963) Petrogenesis of glaucophane schists. Journal of Petrology, 4, 1-30.
635 Ernst, W.G. (1979) Coexisting sodic and calcic amphiboles from relatively high pressure
636 metamorphic belts and the stability of barroisitic amphibole. Mineralogical Magazine, 43,
637 269-278.
638 Etzel, K. and Benisek, A. (2008) thermodynamic mixing behavior of synthetic Ca-

639 Tscheramk-diopside pyroxene solid solutions: III. An analysis of IR line broadening and
640 heat of mixing behavior. Physics and Chemistry of Minerals, 35, 399-407.
641 Gottschalk, M., Andrut, M., and Melzer, S. (1999) The determination of the cummingtonite
642 content of synthetic tremolite. European Journal of Mineralogy, 11, 967-982.
643 Graham, C.M., Maresch, W.V., Welch, M.D., and Pawley, A.R. (1989) Experimental studies
644 on amphiboles: a review with thermodynamic perspectives. European Journal of
645 Mineralogy, 1, 535-555.
646 Hammarstrom, J.M., and Zen, E. (1986) Aluminum in hornblende – An empirical igneous
647 geobarometer. American Mineralogist, 71, 1297-1313.
648 Hawthorne, F.C. and Della Ventura, G. (2007) Short-range order in amphiboles. In,
649 Hawthorne, F.C., Oberti, R., Della Ventura, G., and Mottana, A. (eds) Amphiboles:
650 Crystal Chemistry, Occurrence, and Health Issues, Reviews in Mineralogy and
651 Geochemistry, 67, 173-222.
652 Hawthorne, F.C. and Oberti, R. (2007) Amphiboles: Crystal chemistry. In, F.C. Hawthorne,
653 R. Oberti, G. Della Ventura, and A. Mottana (eds.) Amphiboles: Crystal Chemistry,
654 Occurrence, and Health Issues. Mineralogical Society of America, Reviews in
655 Mineralogy and Geochemistry, 67, p.1-54.
656 Hawthorne, F.C., Welch, M.D., Della Ventura, G., Liu, S., Robert, J.-L., and Jenkins, D.M.
657 (2000) Short-range order in synthetic aluminous tremolite: An infrared and triple-
658 quantum MAS NMR study. American Mineralogist, 85, 1716-1724.
659 Hill, R.J. and Flack, H.D. (1987) The use of the Durbin-Watson *d* statistic in Rietveld
660 analysis. Journal of Applied Crystallography, 20, 356-361.
661 Himmelberg, G.R., and Papike, J.J. (1969) Coexisting amphiboles from blueschist facies
662 metamorphic rocks. Journal of Petrology, 10, 102-114.
663 Hirschmann, M., Evans, B.W., and Yang, H. (1994) Composition and temperature

dependence of Fe-Mg ordering in cummingtonite-grunerite as determined by X-ray diffraction. American Mineralogist, 79, 862-877.

Holland, T. and Blundy, J. (1994) Non-ideal interactions in calcic amphiboles and their bearing on amphibole-plagioclase thermometry. Contributions to Mineralogy and Petrology, 116, 433–447.

Holland, T. and Powell, R. (2003) Activity-composition relations for phases in petrological calculations: an asymmetric multicomponent formulation. Contributions to Mineralogy and Petrology, 145, 492-501.

Hoschek, G. (1995) Stability relations and Al content of tremolite and talc in CMASH assemblages with kyanite + zoisite + quartz + H_2O. European Journal of Mineralogy, 7, 353-362.

Iezzi, G., Della Ventura, G., Tribaudino, M., Nemeth, P., Margiolaki, I., Cavallo, A., Gaillard, F., and Behrens, H. (2010) Phase transition induced by solid solution: The ^{B}Ca-^{B}Mg substitution in richteritic amphiboles. American Mineralogist, 95, 369-381.

Jasmund, K., and Schäfer, R. (1972) Experimentalle Bestimmung der P-T-Stabilitätsreiche in der Mishkristallreihe Tremolit-Tschermakit. Contributions to Mineralogy and Petrology, 34, 101-115.

Jenkins, D.M. (1987) Synthesis and characterization of tremolite in the system H_2O-CaO-MgO-SiO_2. American Mineralogist, 72,707-715.

Jenkins, D.M. (1988) Experimental study of the join tremolite-tschermakite: A reinvestigation. Contributions to Mineralogy and Petrology, 99, 392–400.

Jenkins, D.M. (1994) Experimental reversal of the aluminum content in tremolitic amphiboles in the system H_2O-CaO-MgO-Al_2O_3-SiO_2. American Journal of Science, 294, 593–620.

Jenkins, D.M. (2011) The transition from blueschist to greenschist facies modeled by the

reaction glaucophane + 2 diopside + 2 quartz = tremolite + 2 albite. Contributions to Mineralogy and Petrology, 162, 725–738.

Jenkins, D.M. and Clare, A.K. (1990) Comparison of the high-temperature and high-pressure stability limits of synthetic and natural tremolite. American Mineralogist, 75, 358-366.

Jenkins, D.M. and Corona, J.C. (2006a) The role of water in the synthesis of glaucophane. American Mineralogist, 91, 1055-1068.

Jenkins, D.M. and Corona, J.C. (2006b) Molar volume and thermal expansion of glaucophane. Physics and Chemistry of Minerals, 33, 356-362.

Jenkins, D.M. and Lei, J. (2013) Pressure and temperature variation of octahedral Na and tetrahedral Al in amphiboles in metamafic rocks. American Geophysical Union, Fall Meeting, San Francisco, Abstract V13C-2630.

Jenkins, D.M., Carpenter, M.A., and Zhang, M. (2014) Experimental and infrared characterization of the miscibility gap along the tremolite-glaucophane join. American Mineralogist, 99, 730-741..

Jenkins, D.M., Della Ventura, G., Oberti, R., and Bozhilov, K. (2013) Synthesis and characterization of amphiboles along the tremolite–glaucophane join. American Mineralogist, 98, 588-600.

Larson, A.C. and Von Dreele, R.B. (2000) General Structure Analysis System (GSAS). Los Alamos National Laboratory Report LAUR 86-748.

Lindsley, D.H. and Dixon, S.A. (1976) Diopside-enstatite equilibria at 850° to 1400°C, 5 to 35 kb. American Journal of Science, 276, 1285-1301.

Liou, J.G., Maruyama, S., and Cho, M. (1985) Phase equilibria and mineral parageneses of metabasites in low-grade metamorphism. Mineralogical Magazine, 49, 321-333.

Maresch, W.V., Medenbach, O., and Rudolph, A. (1982) Winchite and the actinolite-glaucophane miscibility gap. Nature, 296, 731-732.

714 Maresch, W.V., Czank, M., and Schreyer, W. (1994) Growth mechanism, structural defects
715 and composition of synthetic tremolite: What are the effects on macroscopic properties?
716 Contributions to Mineralogy and Petrology, 118,297-313

717 Maruyama, S., Cho, M., and Liou, J. (1986) Experimental investigations of blueschist-
718 greenschist transition equilibria: Pressure dependence of Al_2O_3 contents in sodic
719 amphiboles – A new geobarometer. In, B. W. Evans and E. H. Brown (eds.) Blueschists
720 and Eclogites, Geological Society of America, Memoir 164, p. 1-16.

721 Maruyama, S., Liou, J. G., and Terabayashi, M. (1996) Blueschists and eclogites of the world
722 and their exhumation. International Geology Review, 38, 485-594.

723 Najorka, J. and Gottschalk, M. (2003) Crystal chemistry of tremolite-tschermakite solid
724 solutions. Physics and Chemistry of Minerals, 30, 108-124.

725 Newton, R. C. (2011) The three partners of metamorphic petrology. American Mineralogist,
726 96, 457-469.

727 Oberti, R., Hawthorne, F.C., Ungaretti, L., and Cannillo, E. (1995) $^{[6]}$Al disorder in
728 amphiboles from mantle peridotites. Canadian Mineralogist, 33, 867-878.

729 Palin, E.J., Guiton, B.S., Craig, M.S., Welch, M.D., Dove, M.T., and Redfern, S.A.T. (2003)
730 Computer simulation of Al-Mg ordering in glaucophane and a comparison with infrared
731 spectroscopy. European Journal of Mineralogy, 15, 893-901.

732 Papike, J.J., and Clark, J.R. (1968) The crystal structure and cation distribution of
733 glaucophane. American Mineralogist, 53, 1156-1173.

734 Pawley, A.R. (1992) Experimental study of the compositions and stabilities of synthetic
735 nyböite and nyböite-glaucophane amphiboles. European Journal Mineralogy, 4, 171-192.

736 Perdikatsis, B. and Burzlaff, H. (1981) Structurverfeinerung am Talk $Mg_3[(OH)_2Si_4O_{10}]$.
737 Zeitschrift für Kristallographie, 156, 177-186.

738 Powell, R. (1975) Thermodynamics of coexisting cummingtonite-hornblende pairs.

739 Contributions to Mineralogy and Petrology, 51, 29-37.
740 Reynard, B., and Ballèvre, M. (1988) Coexisting amphiboles in an eclogite from the Western
741 Alps: new constraints on the miscibility gap between sodic and calcic amphiboles.
742 Journal of Metamorphic Geology, 6, 333-350.
743 Salje, E.K.H., Carpenter, M.A., Malcherek, T.G.W., and Boffa Ballaran, T. (2000)
744 Autocorrelation analysis of infrared spectra. European Journal of Mineralogy, 12, 503-
745 519.
746 Schmidt, M.W. (1992) Amphibole composition in tonalite as a function of pressure – An
747 experimental calibration of the Al-in-hornblende barometer. Contributions to Mineralogy
748 and Petrology, 110, 304-310.
749 Schumacher, J.C. (2007) Metamorphic amphiboles: Composition and coexistence. In, F.C.
750 Hawthorne, R. Oberti, G. Della Ventura, and A. Mottana (eds.) Amphiboles: Crystal
751 Chemistry, Occurrence, and Health Issues. Mineralogical Society of America, Reviews in
752 Mineralogy and Geochemistry, 67, 359-416.
753 Sharma, A., and Jenkins, D.M. (1999) Hydrothermal synthesis of amphiboles along the
754 tremolite-pargasite join and in the ternary system tremolite-pargasite-cummingtonite.
755 American Mineralogist, 84, 1304-1318.
756 Shirozu, H., and Bailey, S.W. (1966) Crystal structure of a two-layer Mg-vermiculite.
757 American Mineralogist, 51, 1124-1143.
758 Smelik, E.A., and Veblen, D.R. (1992) Exsolution of Ca-amphibole from glaucophane and
759 the miscibility gap between sodic and calcic amphiboles. Contributions to Mineralogy and
760 Petrology, 112, 178-195.
761 Tarantino, S.C., Boffa Ballaran, T., Carpenter, M.A., Domeneghetti, M.A., Tazzoli, V. (2002)
762 Mixing properties of the enstatite–ferrosilite solid solution: II. A microscopic perspective.
763 European Journal of Mineralogy, 14, 537–547.

764 Vernon, R.H. and Clarke, G. (2008) Principles of Metamorphic Petrology. Cambridge
765 University Press, New York, NY, 446 pp.
766 Walker, D. Verma, P.K., Cranswick, L.M.D., Clark, S.M., Jones, R.L., and Buhre, S. (2005)
767 Halite-sylvite thermoconsolution. American Mineralogist, 90, 229-239.
768 Web of Science (2014) Thomson Reuters, Accessed April 14, 2014.
769 Welch, M. D. and Pawley, A. R. (1991) Tremolite: new enthalpy and entropy data from a
770 phase equilibrium study of the reaction tremolite = 2 diopside + 1.5 orthoenstatite + β-
771 quartz + H_2O. American Mineralogist, 76, 1931-1939.
772 Zimmermann, R., Heinrich, W., and Franz, G. (1996) Tremolite synthesis from $CaCl_2$-
773 bearing aqueous solutions. European Journal of Mineralogy, 8, 767-776.
774
775

776 Table 1. Bulk compositions of mixtures investigated in this study.

Sample code prefix	Nominal bulk composition	Components* (mole %)
MgHG-10	$Na_2Mg_3Al_2Si_8O_{22}(OH)_2$	$Hb_0\ Cum_0Tr_0Gl_{100}$
MgHG-9	$Na_{1.8}Ca_{0.185}Mg_{3.125}Al_{1.98}Si_{7.91}O_{22}(OH)_2$	$Hb_9\ Cum_{0.75}Tr_{0.25}Gl_{90}$
MgHG-5	$Na_{1.6}Ca_{0.37}Mg_{3.25}Al_{1.96}Si_{7.82}O_{22}(OH)_2$	$Hb_{18}\ Cum_{1.5}Tr_{0.5}Gl_{80}$
MgHG-3	$Na_{1.4}Ca_{0.555}Mg_{3.375}Al_{1.94}Si_{7.73}O_{22}(OH)_2$	$Hb_{27}\ Cum_{2.25}Tr_{0.75}Gl_{70}$
MgHG-7	$Na_{1.2}Ca_{0.74}Mg_{3.5}Al_{1.92}Si_{7.64}O_{22}(OH)_2$	$Hb_{36}\ Cum_3Tr_1Gl_{60}$
MgHG-1	$Na_{1.0}Ca_{0.925}Mg_{3.625}Al_{1.90}Si_{7.55}O_{22}(OH)_2$	$Hb_{45}\ Cum_{3.75}Tr_{1.25}Gl_{50}$
MgHG-6	$Na_{0.8}Ca_{1.11}Mg_{3.75}Al_{1.88}Si_{7.46}O_{22}(OH)_2$	$Hb_{54}\ Cum_{4.5}Tr_{1.5}Gl_{40}$
MgHG-2	$Na_{0.6}Ca_{1.295}Mg_{3.875}Al_{1.86}Si_{7.37}O_{22}(OH)_2$	$Hb_{63}\ Cum_{5.25}Tr_{1.75}Gl_{30}$
MgHG-4	$Na_{0.4}Ca_{1.48}Mg_4Al_{1.84}Si_{7.28}O_{22}(OH)_2$	$Hb_{72}\ Cum_6Tr_2Gl_{20}$
MgHG-8	$Na_{0.2}Ca_{1.665}Mg_{4.125}Al_{1.82}Si_{7.19}\ O_{22}(OH)_2$	$Hb_{81}\ Cum_{6.75}Tr_{2.25}Gl_{10}$
MgHG-11(=A)	$Ca_{1.85}Mg_{4.25}Al_{1.80}Si_{7.10}O_{22}(OH)_2$	$Hb_{90}\ Cum_{7.5}Tr_{2.5}Gl_0$

777 *Component abbreviations and compositions: Hb (Hornblende) =

778 $Ca_2(Mg_4Al)(AlSi_7)O_{22}(OH)_2$; Cum (Cummingtonite) = $Mg_7Si_8\ O_{22}(OH)_2$; Tr (Tremolite) =

779 $Ca_2Mg_5Si_8\ O_{22}(OH)_2$; Gl (Glaucophane) = $Na_2(Mg_3Al_2)Si_8O_{22}(OH)_2$

780 Table 2. Treatment conditions and products of synthesis for mixtures investigated on the
781 hornblende-glaucophane join

Sample Code	Nominal Gl (mol %)	*T* (°C)	*P* (GPa)	*t* (h)	H_2O[c] (wt%)	Products
MgHG-10-2.2[a]	100	760(10)	2.50(3)	116.8	0	amph (99%), talc (1%)
MgHG-(R)9	90	755(20)	2.34(3)	72.0	0	amph (99.8%), smec (0.2%)
MgHG-(R)5-2.2[a]	80	750(10)	2.25(3)	144.0	0	amph (99%), talc (1%)
MgHG-3.3[b]	70	735(10)	1.8(3)	215.8	0	amph (92%), qtz (8%)
MgHG-(R)7-2.2[a]	60	790(10)	2.12(3)	96.0	0	amph (95%), talc (4.5%, smec (0.5%), liq
MgHG-1.2[a]	50	755(5)	2.00(3)	168.2	2.03	amph (97%), talc (3%)
MgHG-(R)6	40	805(20)	2.00(3)	72.0	0	amph (92%), talc (8%)
MgHG-2	30	760(10)	2.00(3)	71.3	0	amph (96%), talc (4%)
MgHG-(R)4-2	20	830(10)	1.50(3)	72.0	0	amph (100%)
MgHG-(R)8-2	10	830(10)	1.50(3)	72.0	0	amph (100%)
MgHG-11	0	860(20)	1.29(3)	72.0	0	amph (100%)

782 Note: Uncertainties in last digit shown in parentheses. Proportions (wt%) of products are
783 from the Rietveld refinements and involve only the crystalline phases. . Abbreviations:
784 amph = amphibole; qtz = quartz; smec = smectite; liq = quenched liquid or aqueous solute
785 [a] Retreatment of the previous synthesis, with intermediate grinding, at the same conditions.
786 Time shown is the cumulative duration of both treatments.
787 [b] This sample was treated three separate times, with intermediate grinding. Time shown is the
788 total duration of all treatments.
789 [c] H_2O added to the starting mixture. For most experiments water is introduced as $Mg(OH)_2$

790 Table 3. Compositions of amphiboles synthesized in this study, reported as the average of *n*

791 analyses, given in weight%, cations per 23 oxygens, and cation site occupancies.

Sample	MgHG-10-2.2	MgHG-(R)9	MgHG-(R)5-2.2	MgHG-3.3	MgHG-(R)7-2.2
	100 (Gl, mol%)	90	80	70	60
n	3	15	15	8	14
weight %					
SiO_2	46.9(17)	58.1(10)	50.3(41)	57.5(12)	55.1(14)
Al_2O_3	9.5(3)	13.4(6)	11.8(11)	13.1(4)	12.4(8)
MgO	12.8(11)	16.2(11)	16.0(18)	18.9(9)	19.6(12)
CaO	0.08(5)	1.6(3)	2.7(4)	4.3(5)	6.2(7)
Na_2O	5.6(1)	7.8(5)	5.5(7)	5.8(3)	4.6(7)
Total	75.0(28)	97.2(14)	86.3(77)	99.7(15)	97.9(9)
cations					
Si	7.97(2)	7.71(10)	7.54(8)	7.49(10)	7.35(12)
Al	1.91(8)	2.10(9)	2.08(5)	2.01(4)	1.95(12)
Mg	3.25(18)	3.20(20)	3.56(13)	3.67(17)	3.89(25)
Ca	0.02(1)	0.23(4)	0.44(4)	0.60(7)	0.89(10)
Na	1.84(7)	2.00(12)	1.61(10)	1.46(6)	1.18(17)
Total	14.99(2)	15.24(12)	15.23(11)	15.24(11)	15.26(13)
site occupancies					
^{T}Si	7.97(2)	7.71(10)	7.54(8)	7.49(10)	7.35(12)
^{T}Al	0.03(2)	0.29(10)	0.46(8)	0.51(10)	0.65(12)
^{C}Al	1.88(9)	1.81(11)	1.62(8)	1.50(12)	1.30(15)
^{C}Mg	3.12(9)	3.16(16)	3.38(8)	3.50(12)	3.69(17)
^{B}Mg	0.13(9)	0.04(6)	0.18(6)	0.17(5)	0.20(10)
^{B}Ca	0.02(1)	0.23(4)	0.44(4)	0.60(7)	0.89(10)
^{B}Na	1.84(8)	1.73(7)	1.38(7)	1.23(11)	0.91(15)
^{A}Na	0.00	0.28(12)	0.23(11)	0.24(11)	0.27(12)

792

793

794 Table 3- continued

Sample	MgHG-1.2	MgHG-(R)6	MgHG-2	MgHG-(R)4-2	MgHG-(R)8-2	MgHG-11
	50	40	30	20	10	0
n	10	15	10	18	16	23
weight%						
SiO_2	51.8(16)	52.9(8)	53.8(17)	52.8(10)	49.1(32)	51.9(11)
Al_2O_3	11.6(12)	12.3(5)	11.4(25)	11.1(11)	10.7(13)	11.6(7)
MgO	19.8(9)	20.1(4)	20.6(7)	21.6(9)	20.1(16)	21.1(6)
CaO	7.7(4)	9.2(3)	9.6(4)	11.0(6)	11.0(10)	12.1(9)
Na_2O	3.5(3)	2.9(2)	2.3(4)	1.3(2)	0.68(7)	0.02(2)
Total	94.4(31)	97.4(9)	97.7(13)	97.8(16)	91.6(61)	96.8(14)
cations						
Si	7.21(7)	7.15(6)	7.24(22)	7.12(8)	7.08(10)	7.07(8)
Al	1.90(16)	1.96(8)	1.80(39)	1.77(17)	1.82(17)	1.86(12)
Mg	4.11(13)	4.04(9)	4.14(14)	4.35(16)	4.32(10)	4.28(11)
Ca	1.15(7)	1.33(4)	1.38(5)	1.58(8)	1.70(11)	1.77(14)
Na	0.94(8)	0.77(4)	0.60(10)	0.34(4)	0.19(2)	0.007(6)
Total	15.31(5)	15.25(5)	15.16(7)	15.17(7)	15.11(4)	14.99(4)
site occupancies						
^{T}Si	7.21(7)	7.15(6)	7.24(22)	7.12(8)	7.08(10)	7.07(8)
^{T}Al	0.79(7)	0.85(6)	0.76(22)	0.88(8)	0.92(10)	0.92(8)
^{C}Al	1.11(12)	1.11(6)	1.04(17)	0.89(12)	0.90(9)	0.94(7)
^{C}Mg	3.89(12)	3.89(6)	3.96(17)	4.11(12)	4.10(9)	4.06(7)
^{B}Mg	0.22(4)	0.16(5)	0.18(7)	0.24(8)	0.21(11)	0.22(11)
^{B}Ca	1.15(8)	1.33(4)	1.38(5)	1.58(8)	1.70(11)	1.77(14)
^{B}Na	0.63(8)	0.52(4)	0.44(6)	0.17(7)	0.08(4)	0.005(5)
^{A}Na	0.31(5)	0.25(5)	0.16(7)	0.17(7)	0.11(4)	0.002(5)

795 Note: Uncertainties (1σ) in the last digit are given in parentheses.
796

797 Table 4. Unit-cell dimensions of synthetic amphibole made in this study and selected whole-pattern agreement indices.

Sample Code	Bulk Ca, apfu	*a*, Å	*b*, Å	*c*, Å	β, °	*V*, Å^3	*GoF*	DW-*d*	R_{wp}
MgHG-10-2.2	0.02(1)	9.5381(7)	17.698(2)	5.2892(4)	103.540(8)	868.0(1)	1.36	1.19	19.9
MgHG-(R)9	0.23(4)	9.5752(8)	17.735(2)	5.2872(6)	103.69(1)	872.3(1)	1.41	1.14	21.1
MgHG-(R)5-2.2	0.44(4)	9.6173(9)	17.764(2)	5.2882(6)	103.95(1)	876.8(1)	1.31	1.39	23.4
MgHG-3.3	0.60(7)	9.652(1)	17.790(2)	5.2869(6)	104.15(1)	880.3(1)	1.44	1.17	24.5
MgHG-(R)7-2.2	0.89(10)	9.734(1)	17.885(2)	5.2814(5)	104.44(1)	890.4(1)	1.35	1.33	19.4
MgHG-1.2	1.15(8)	9.7427(6)	17.896(2)	5.2815(6)	104.564(8)	891.3(1)	1.44	1.17	17.5
MgHG-(R)6	1.33(4)	9.7617(4)	17.917(1)	5.2817(4)	104.731(5)	893.45(7)	1.54	1.04	14.8
MgHG-2	1.38(5)	9.7736(6)	17.949(2)	5.2828(6)	104.751(7)	896.2(1)	1.35	1.26	21.9
MgHG-(R)4-2	1.58(8)	9.7793(6)	17.976(2)	5.2824(6)	104.841(7)	897.6(1)	1.25	1.57	22.4
MgHG-(R)8-2	1.70(11)	9.7681(4)	17.974(1)	5.2843(3)	104.874(5)	896.70(7)	1.68	0.94	16.2
MgHG-11	1.77(14)	9.7517(6)	17.982(2)	5.2867(5)	104.868(7)	896.0(1)	1.69	0.83	26.1

798 Note: Uncertainties in the last digit (1σ) given in parentheses. The whole-pattern refinement indices are: GoF is Goodness of Fit =

799 $R_{wp}/R_{exp} = \sqrt{\chi^2}$; DW-*d* is the Durbin-Watson *d* statistic (Hill and Flack, 1987), R_{wp} = weighted pattern agreement index (with

800 background). The unit-cell parameters of *a*, *b*, *c*, *β* and volume (*V*) were derived with halite as an internal standard.

801

802

Table 5. Compositions of amphiboles from Table 3 recast into the mole fractions of Gl, Hb, Cm, and Kt, the corrected composition Hb', and the corresponding corrected volume *V*corr.

Sample Code	Amphibole Components (mole fractions)					V_{obs} (Å^3)	V_{corr} (Å^3)
	Gl	Hb	Cm	Kt	Hb'		
MgHG-10-2.2	0.94(4)	0.005(4)	0.05(4)	0.001(3)	0.005(5)	868.0(1)	866(12)
MgHG-(R)9	0.72(8)	-0.02(5)	0.02(3)	0.28(12)	-0.05(10)	872.3(1)	863(6)
MgHG-(R)5-2.2	0.58(8)	0.10(5)	0.09(3)	0.23(11)	0.14(5)	876.8(1)	871(4)
MgHG-3.3	0.49(10)	0.18(4)	0.09(2)	0.24(11)	0.27(4)	880.3(1)	876(3)
MgHG-(R)7-2.2	0.32(10)	0.31(7)	0.10(5)	0.27(12)	0.50(9)	890.4(1)	892(2)
MgHG-1.2	0.16(6)	0.42(4)	0.11(2)	0.31(5)	0.73(7)	891.3(1)	893.6(8)
MgHG-(R)6	0.13(4)	0.54(3)	0.08(2)	0.25(5)	0.80(4)	893.45(7)	895.9(8)
MgHG-2	0.14(4)	0.61(5)	0.09(3)	0.16(7)	0.81(4)	896.2(1)	899(2)
MgHG-(R)4-2	0.00(6)	0.71(5)	0.12(4)	0.17(7)	1.00(10)	897.6(1)	903(3)
MgHG-(R)8-2	-0.01(4)	0.79(6)	0.11(6)	0.11(4)	1.02(5)	896.70(7)	900(2)
MgHG-11	0.002(4)	0.88(7)	0.11(6)	0.002(5)	0.99(2)	896.0(1)	903(20)

Note: Mole fractions of the amphibole components were calculated from the analyses given in Table 3 as follows: Gl = (^{B}Na-^{A}Na)/2, Hb = (^{B}Ca-^{A}Na)/2, Cm = ^{B}Mg/2, Kt = ^{A}Na. Hb' is the mole fraction of Hb excluding Cm or Kt components. V_{obs} is the observed unit-cell volume (Table 4) while V_{corr} is the volume corrected back to the Hb-Gl join using Equation 1 in the text. Uncertainty in the last digit is shown in parentheses.

Table 6. Treatment conditions and re-equilibration products of coexisting glaucophane and magnesio-hornblende "A" mixed in a molar ratio of 1:1 and treated for different durations.

Sample code	*T* (°C)	*P* (GPa)	t (h)	H_2O (wt%)	Products
MgHG-M_3	600(5)	2.00(3)	143.6	3	Gl-amph, Hb-amph, talc
MgHG-M_3-2*	600(5)	2.00(3)	258.9	3	Gl-amph, Hb-amph, talc, qtz(?)
MgHG-M_5	650(5)	2.02(3)	166.5	3	Gl-amph, Hb-amph, smec, qtz
MgHG-M_5-2*	650(5)	2.02(3)	338.5	3	Gl-amph, Hb-amph, qtz, talc
MgHG-M_2	700(5)	2.00(5)	119	3	Gl-amph, Hb-amph, qtz
MgHG-M_2-2*	700(5)	2.00(5)	238	3	Gl-amph, Hb-amph, qtz
MgHG-M_2-3*	700(5)	2.00(5)	356.8	3	Gl-amph, Hb-amph, smec, qtz
MgHG-M_2-4*	700(5)	2.00(5)	476.8	3	amph, qtz, smec
MgHG-M_4	750(5)	2.07(3)	159.4	3	amph, talc
MgHG-M_4-2*	750(5)	2.07(3)	201.3	3	amph, talc
MgHG-M_1	800(5)	2.00(5)	71	3	amph

Note: Uncertainties in last digit are shown in parentheses. Gl-amph = Gl-rich amphibole, Hb-amph = Hb-rich amphibole. Other abbreviations as in Table 2.

* Retreatment of the previous treatment with intermediate grinding. Time shown is the cumulative duration.

818 Table 7. Amphibole volumes and corresponding compositions from the re-equilibration
819 experiments reported in Table 6.

Sample code	Temp (°C)	Volume		Composition (Ca,apfu)	
		Gl	Hb	Gl	Hb
MgHG-mixture	------	867.8(1)	894.5(1)	0.09(2)	1.36(13)
MgHG-M_3-1	600	870.66(2)	895.4(2)	0.18(3)	1.45(15)
MgHG-M_3-2*	600	866.7(3)	892.2(3)	0.06(2)	1.16(11)
MgHG-M_5-1	650	869.65(3)	892.83(2)	0.15(3)	1.20(11)
MgHG-M_5-2*	650	864.1(3)	891.8(3)	-0.02(2)	1.13(10)
MgHG-M_2-1	700	869.59(3)	891.6(2)	0.15(3)	1.11(10)
MgHG-M_2-2*	700	884.24(3)	893.17(2)	0.70(7)	1.23(12)
MgHG-M_2-3*	700	884.91(3)	891.6(3)	0.73(7)	1.12(10)
MgHG-M_2-4*	700	884.0(3)	----------	0.69(6)	----------
MgHG-M_4-1	750	881.9(4)	892.5(6)	0.60(6)	1.18(11)
MgHG-M_4-2*	750	----------	888.3(2)	----------	0.91(8)
MgHG-M_1	800	----------	883.4(2)	----------	0.66(6)

820 Uncertainties in last digit shown in parentheses.
821 * Retreatment of the previous treatment with intermediate grinding. Time shown is the
822 cumulative duration.

823 Table 8. Modeled component band positions (cm^{-1}) and relative intensities in the OH-stretching
824 region.

Sample code	Nom. Gl	Band Position and Relative Intensities					
	(mole %)	A'	A	B	B’	C	D
MgHG-10-2.2	Gl_{100}	-------	-------	3664	3673	-------	-------
				0.583	0.417		
MgHG-(R)9	Gl_{90}	3638	3653(?)	3664	-------	3681	-------
		0.156	0.008	0.798		0.038	
MgHG-(R)5-2.2	Gl_{80}	3640	-------	3665	-------	3686	3724
		0.059		0.762		0.006	0.173
MgHG-3.2	Gl_{70}	3646	3654	3665	-------	3685	3713
		0.128	0.010	0.571		0.037	0.254
MgHG-1.2	Gl_{50}	-------	3655	3676	-------	3692	3713
			0.438	0.351		0.046	0.165
MgHG-2	Gl_{30}	-------	3658	3673	-------	3700	3714
			0.581	0.312		0.039	0.068
MgHG-(R)4-2	Gl_{20}	-------	3655	3672	-------	3693	3709
			0.467	0.409		0.020	0.104
MgHG-(R)8-2	Gl_{10}	-------	3651	3670	-------	3686	3742
			0.465	0.505		0.018	0.013

825

826

827 Table 9. Macroscopic interaction parameters (W_i) and size parameters (α_i) from this study and
828 that of Diener and Powell (2012)

Parameter	This study	Diener & Powell (2012)
$W_{Gl,Tr}$, kJ	70[a]	65
$W_{Gl,Ts}$, kJ	20	25
$W_{Tr,Ts}$, kJ	20	20
α_{Gl}	0.52[a]	0.8
α_{Tr}	1.0	1.0
α_{Ts}	1.2	1.5

829 [a] Values based on the tremolite–glaucophane join (Jenkins et al. 2014)

830

831

Figure Captions

Figure 1. Powder XRD patterns of selected samples. (a) Powder XRD pattern obtained for $Hb_{81}Mc_{6.75}Tr_{2.25}G_{10}$ (MgHG-(R)8-2, Table 2) made at 830°C, 1.5GPa, for 72 hours. The pattern shows essentially a pure yield of amphibole. (b) Powder XRD pattern obtained for $Hb_{36}Mc_3Tr_1Gl_{60}$ (MgHG-(R)7-2.2, Table 2) made at 790°C , 2.12GPa, for 96 hours. The major peaks of non-amphibole phases (smectite, talc) are indicated, while the slightly elevated background in this pattern relative to that in (a) suggests a small proportion of amorphous material is present, labeled here as Liq.

Figure 2. (a) Compositions of amphiboles synthesized in this study (open circles) at 10 mol% increments along the join "A"–Gl shown in the tretrahedron Na_2O-CaO-MgO-Al_2O_3 projected from SiO_2 and H_2O. The compositions of these samples are closely modeled by the amphibole tetrahedron magnesio-hornblende (Hb), cummingtonite (Cm), glaucophane (Gl), and katophorite (Kt). (b) Same amphibole compositions as shown in (a) but projected from $Mg_7Si_8O_{22}(OH)_2$ (cummingtonite), SiO_2, and H_2O onto the tshermakite(Ts)–tremolite(Tr)–Gl ternary plane. Representative error in the projected compositions is shown.

Figure 3. Back-scattered electron images of representative samples of the amphiboles synthesized in this study. (a) Sample MgHG-1.2 (nominal Gl_{50}) treated at 755 °C and 2.0 GPa for 168 h. The amphibole (medium grey) constitutes about 97 wt% (Table 2) of this sample with talc (darker grey, matrix) being about 3 wt%. Amphibole occurs in a range of sizes with the largest grain at lower center being about 10 μm long and 3 μm wide. Scale is 10 μm. (b) Sample MgHG-10-2.2 (nominal Gl_{100}) treated at 760 °C and 2.5 GPa for 117 h. This sample shows the very fine-grained texture of pure glaucophane; the large bright areas are aggregates of fine grains. Scale is 20 μm. (c) Sample MgHG-11 (nominal Gl_0) treated at 860 °C and 1.3 GPa for 72 h. Pure "A" amphibole forms as numerous needles and elongate

laths. Box is the area shown in (d). Scale is 20 μm. (d) Enlargement of the central area of (c) showing the distinctly larger grain size of Hb-rich amphiboles, some reaching 25 μm long by 3 μm wide. Scale is 5 μm.

Figure 4. (a) Open circles are the unit-cell dimensions [a, b, c, (Å), β (°), and V (Å^3)] plotted as a function of the observed Ca contents (apfu) from electron microprobe analysis (EMPA, Table 3). Curve shown for the volumes is a second-order polynomial, indicated on the figure, fitted to the open circles and the volume for end-member glaucophane (solid circle) from Jenkins and Corona (2006). Shown for comparison are the volumes for magnesio-hornblende extrapolated from the data of Najorka and Gottschalk (2003, NG2003), and from the equations given by Hawthorne and Oberti (2007, HO2007). (b) Volumes corrected for the components Cm and Kt using Equation (1) as described in the text and projected onto the Hb-Gl join. Solid curve is a polynomial fit to the corrected volumes (V_{corr}) and weighted by the inverse of the uncertainty of each volume. Data are taken from Table 5. Dashed line is the same curve shown in (a) provided for comparison. Other symbols as in (a).

Figure 5. Amphibole re-equilibration experiments involving the dissolution of Hb-rich amphibole (solid circles) and Gl-rich amphibole (open circles) as a function of time. (a) Results at 600°C and 2 GPa (MgHG-M3-series, Table 6). (b) Results at 650°C and 2 GPa (MgHG-M5-series, Table 6). (c) Results at 700°C and 2 GPa (MgHG-M2-series, Table 6). Note the convergence to a single amphibole at 700°C.

Figure 6. Powder XRD patterns showing the homogenization of glaucophane and amphibole "A" into a single amphibole in the time-series experiments done at 700°C and 2 GPa for a total of 477 h (MgHG-M_2-series, Table 7). Vertical arrows and dashed lines indicate the location of several free-standing XRD peaks of glaucophane, labeled with the corresponding

879 indices, in the starting mixture. By the last treatment (MgHG-M_2-4) there is essentially one
880 amphibole present.

881 Figure 7. Temperature-composition diagram showing the amphibole re-equilibration results
882 (Table 7). Small dots indicate the starting compositions of the amphiboles, the open circles
883 are the compositions of Gl-rich amphiboles, and open squares are the compositions of Hb-
884 rich amphiboles. Arrows indicate the sense of compositional re-equilibration. Miscibility
885 gap separating the fields of one- and two- amphibole stability is a binary section through the
886 ternary amphibole system Gl-Tr-Ts as discussed in the text. The solid curve shown here is
887 represented by the following 4^{th}-order polynomial: $T(°C) = 370.70 + 1535.32 \cdot (Ca, apfu) -$
888 $2558.81 \cdot (Ca^2) + 1653.95 \cdot (Ca^3) - 411.53 \cdot (Ca^4)$.

889 Figure 8. Infrared spectra in the MIR range of the amphiboles formed in this study, labeled with
890 the nominal mol% of the Gl component.

891 Figure 9. Infrared spectra in the FIR range of the amphiboles formed in this study, labeled with
892 the nominal mol% of the Gl component.

893 Figure 10. Plot of the autocorrelation band-width parameter $\Delta corr_i$ versus the observed Ca
894 cations (apfu) for four regions of the MIR spectra: (a) 162–224 cm^{-1} (= 200 cm^{-1}), (b) 328–
895 407 cm^{-1} (= 360 cm^{-1}), (c) 410–610 cm^{-1} (= 500 cm^{-1}), and (d) 620–1300 cm^{-1} (= 800 cm^{-1}).

896 Figure 11. Values of $\delta\Delta corr_i$ derived from the data in Figure 10 plotted against the observed Ca
897 (apfu). The data in (a) and (d) were fitted to an asymmetric two-parameter expression similar
898 to that used to model enthalpy of mixing and the derived parameters are listed on the plot.
899 The data in (b) and (c) are too scattered to permit any simple fit.

900 Figure 12. Infrared spectra in the OH-stretching region of selected synthetic amphiboles from
901 this study labeled with the sample codes and nominal mol% Gl component. The observed

intensitites are represented by dots while the modeled intensities are shown by a solid curve. The broad absorption band centered near 3500 cm^{-1} is attributed to moisture absorbed by the sample. Locations of main band components are shown by letters.

Figure 13. (a) Compositions of coexisting amphiboles along the join "A"-glaucophane from this study and along the join tremolite-glaucophane from the study of Jenkins et al. (2014). Legend indicates the temperatures of the coexisting amphiboles. Star is the composition of ideal magnesio-hornblende. Solid curves are calculated isotherms of the two-amphibole field as discussed in the text. (b) Calculated isothermal section at 500 °C showing the sense of the tie-lines.

Figure 14. Calculated excess Gibbs free energy (G^{excess}) along the magnesio-hornblende–glaucophane join using the size parameters (α_i) and macroscopic interaction parameters ($W_{i,j}$) from this study (Table 9) and equation 7.

Figre 15. (a) Figure showing the correlation between ^{B}Na and ^{T}Al for amphiboles coexisting with albite, chlorite, and iron oxide after Figure 10 of Brown (1977). Locality abbreviations are: Shuksan = northern Cascades, Washington; Sanbagawa = Sanbagawa terrane, central Shikoku, Japan; Otago = metamorphic terrane of western Otago, south island, New Zealand; and Sierra = contact aureoles of Sierra Nevada, California. (b) Isotherms of the miscibility gap shown in Figure 13a superimposed on the compositional plot of Brown (1977). Note the close agreement between the amphibole compositions and the location of the miscibility gap, particularly at the lower temperature range, suggesting that temperature, rather than pressure, has the dominant control on amphibole compositions.

924

925 Figure 1

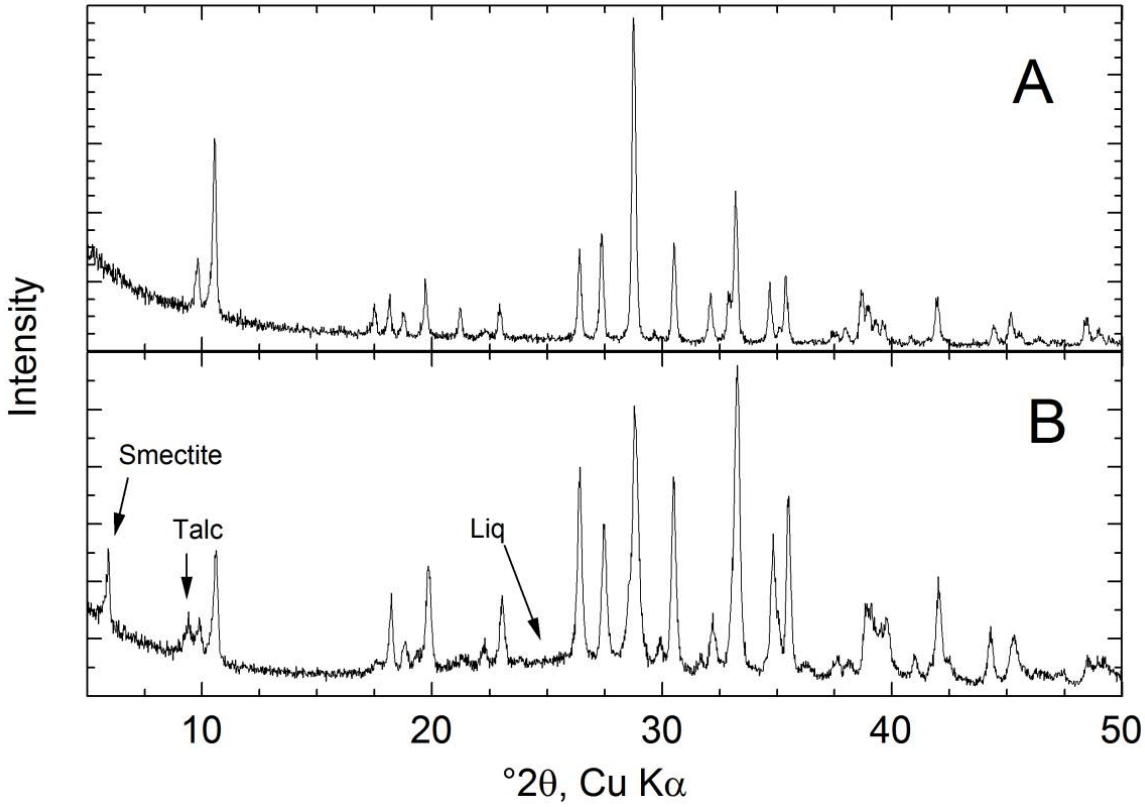

926

927

928

929 Figure 2

930

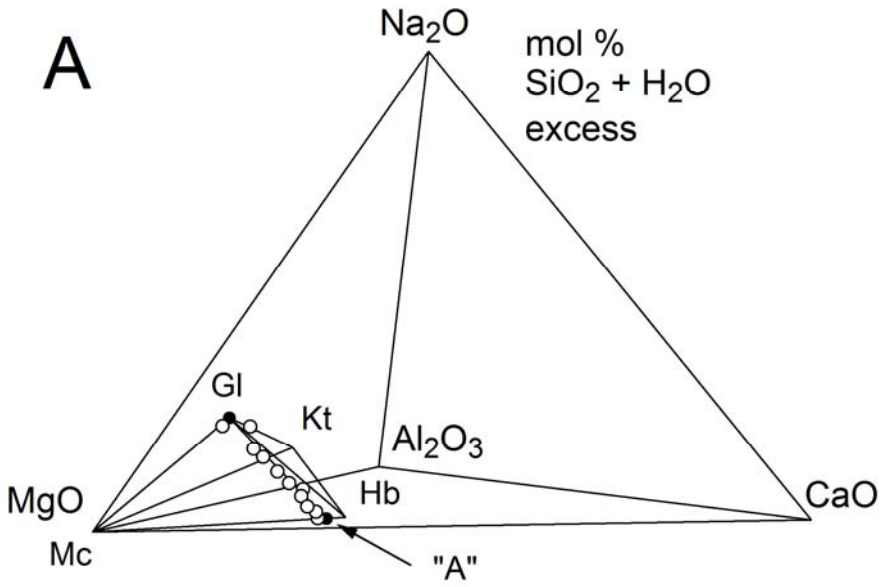

931
932

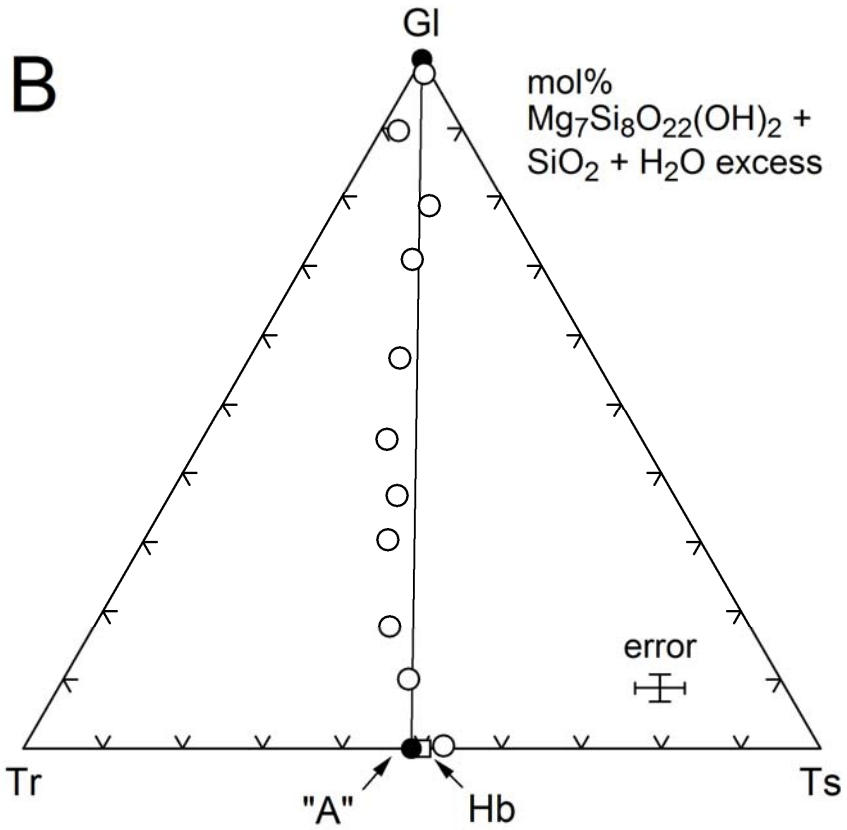

933

934 Figure 3

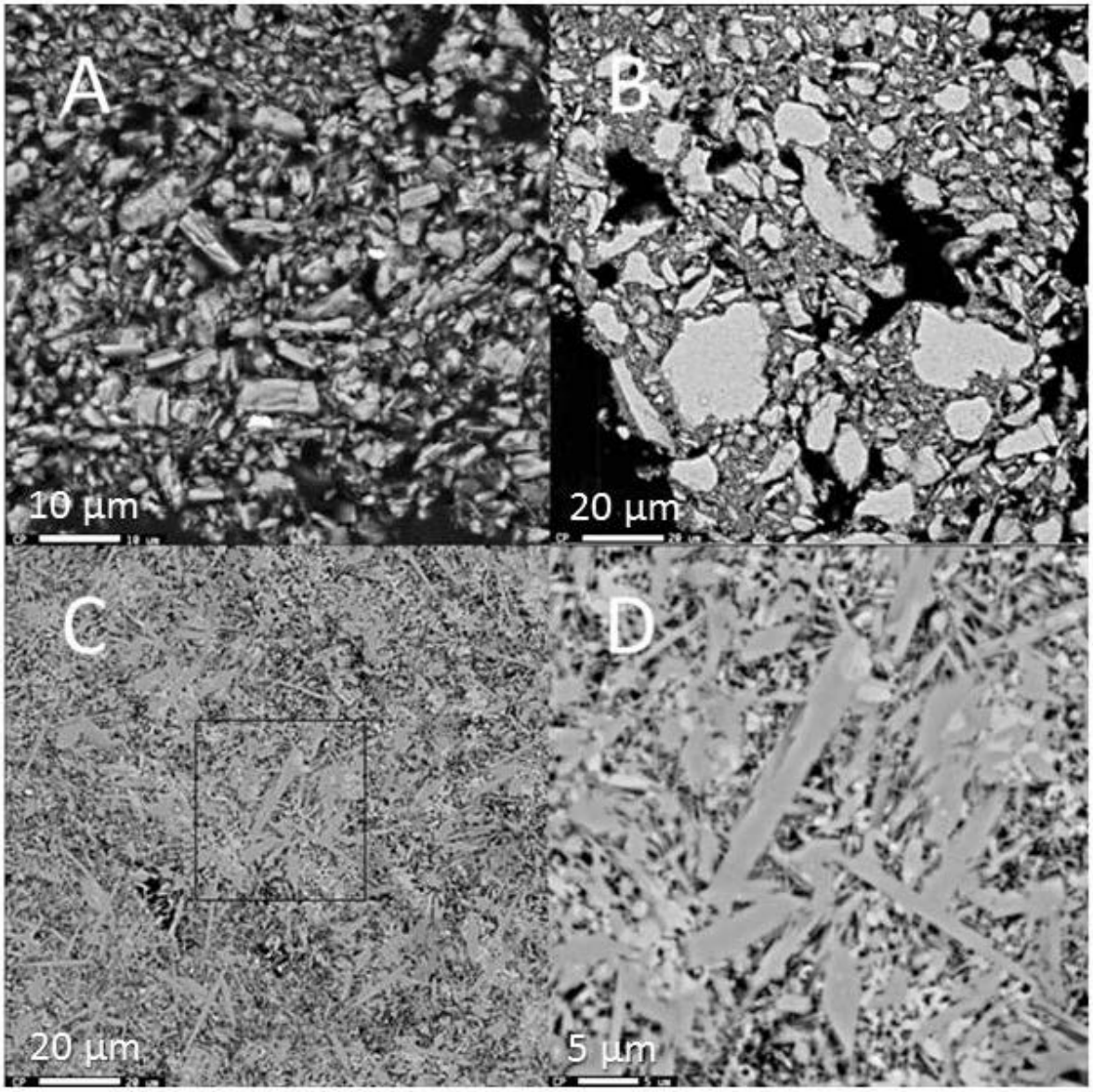

935

936

937 Figure 4
938

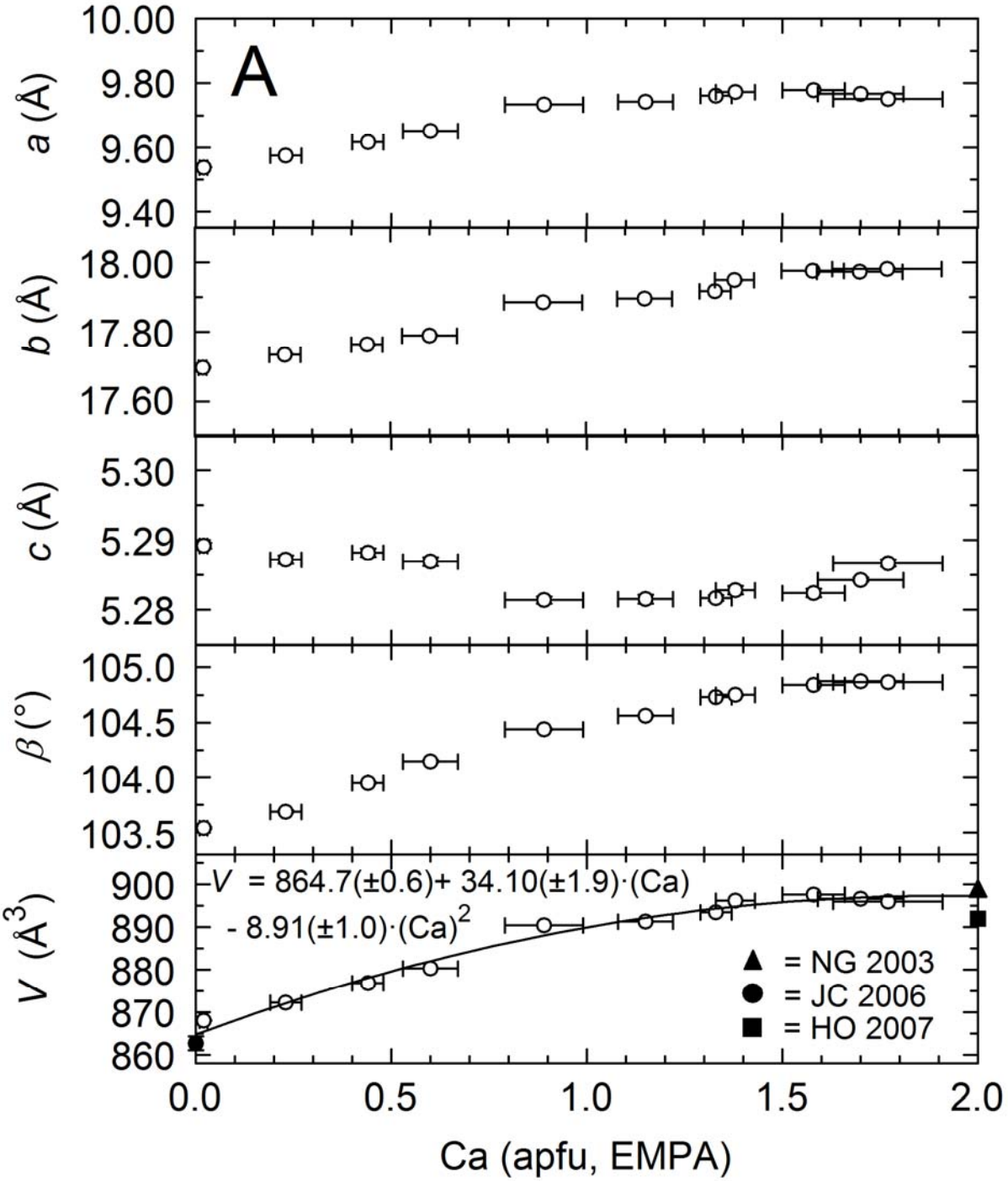

939
940
941
942

943 Figure 4
944

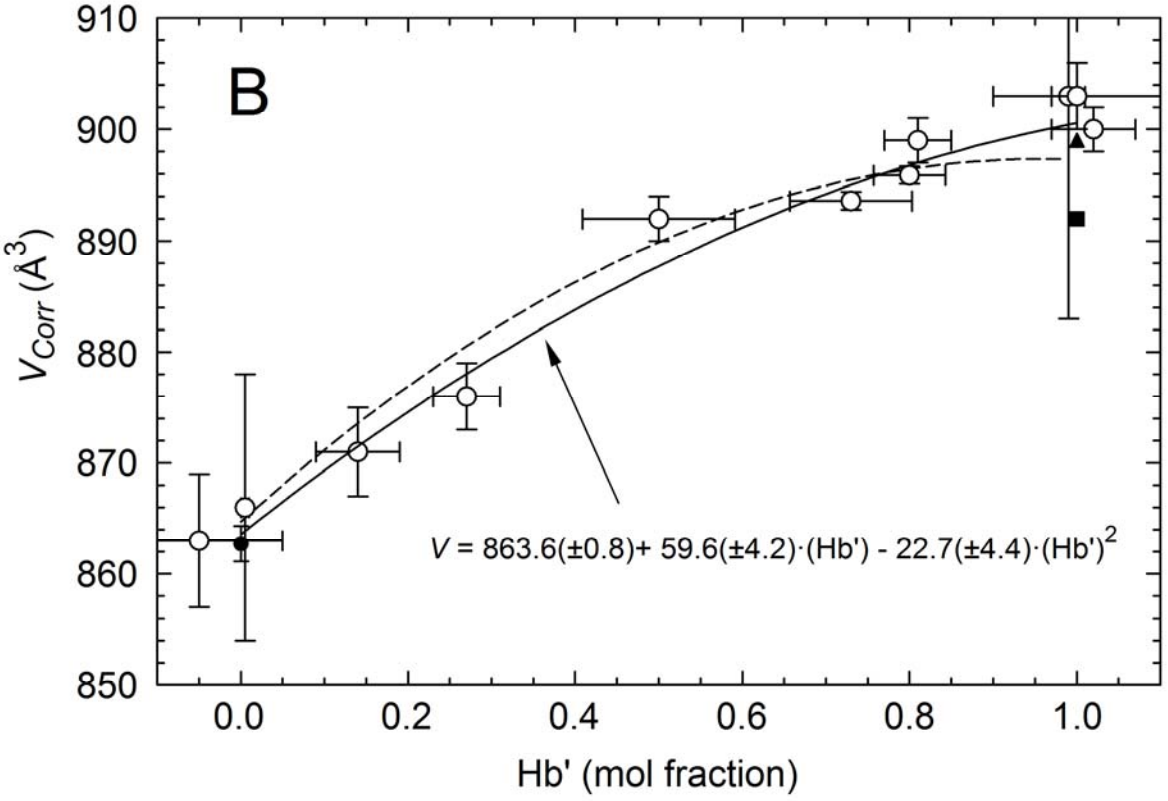

945
946
947

948
949 Figure 5
950

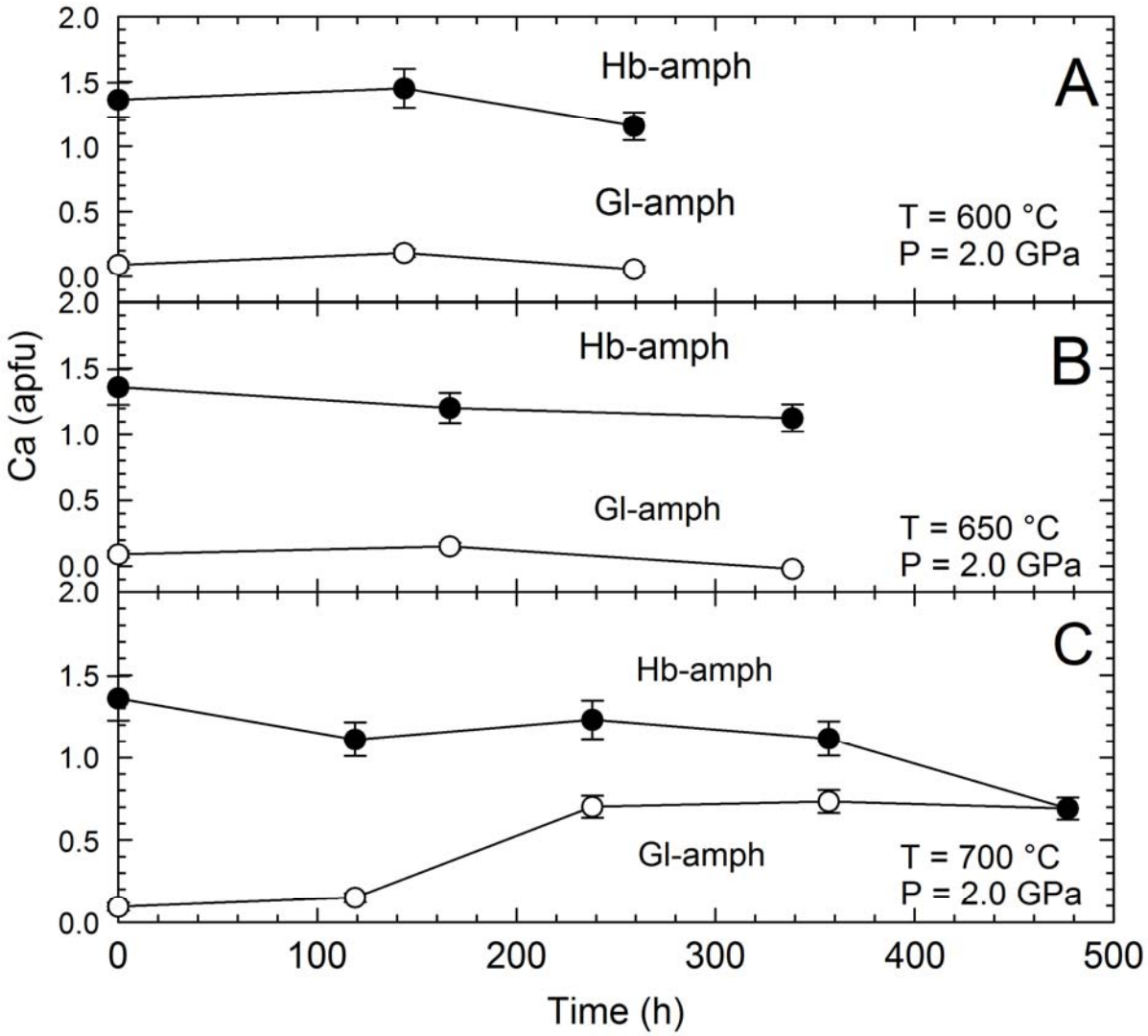

951

952

953

954 Figure 6

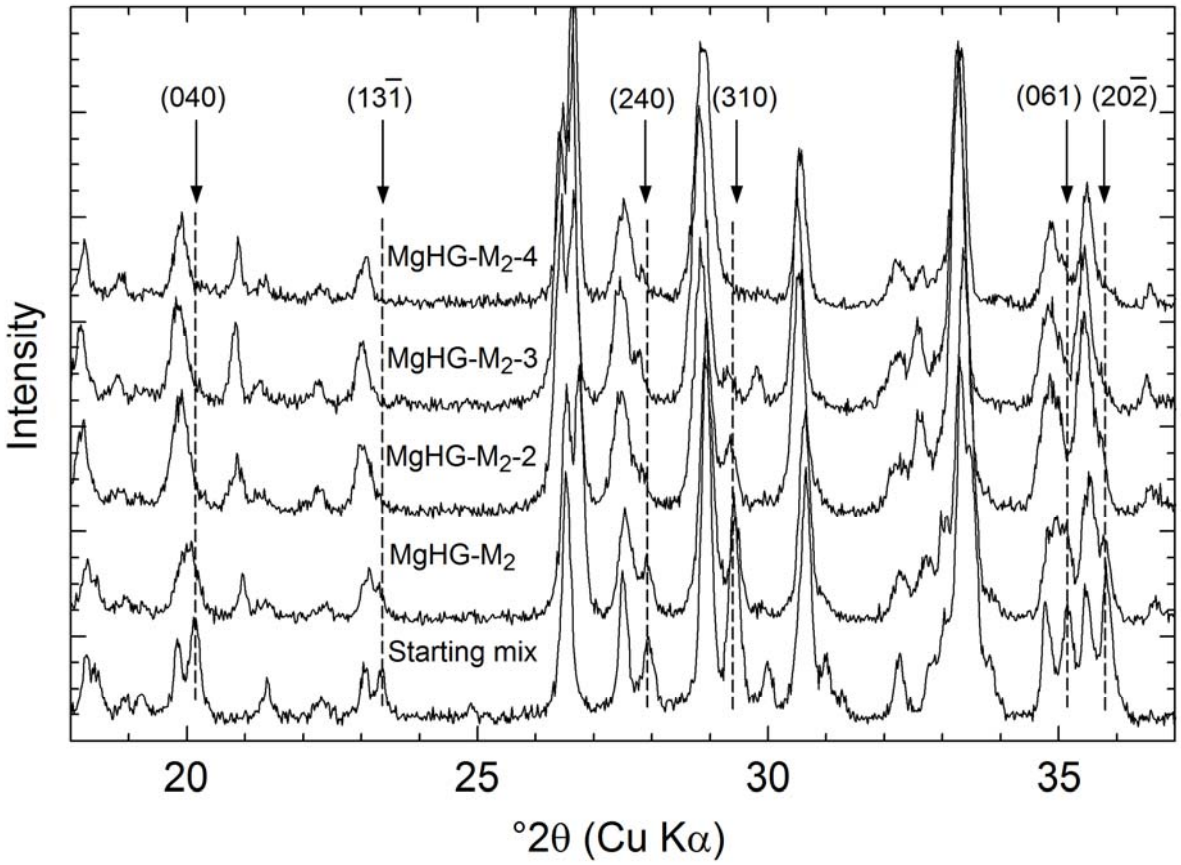

955

956

957 Figure 7

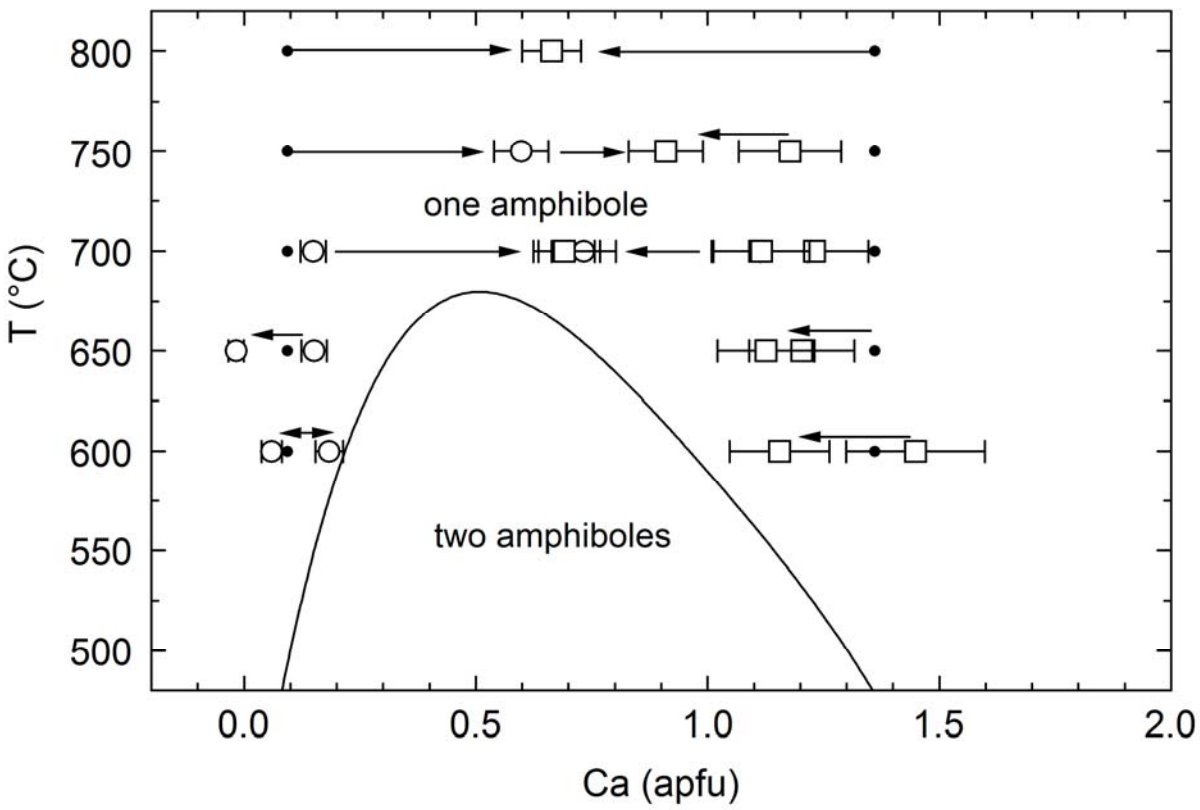

958

959

960 Figure 8

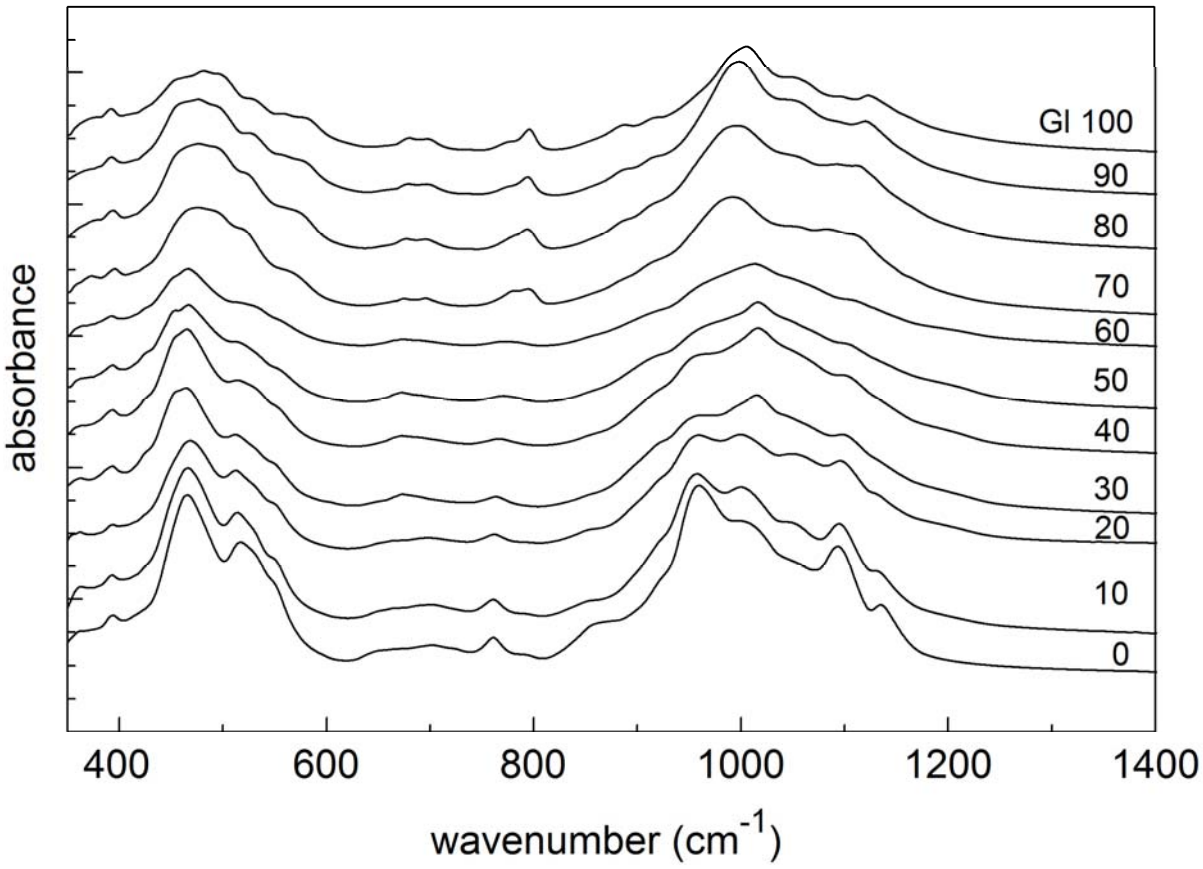

961

962

963

964 Figure 9

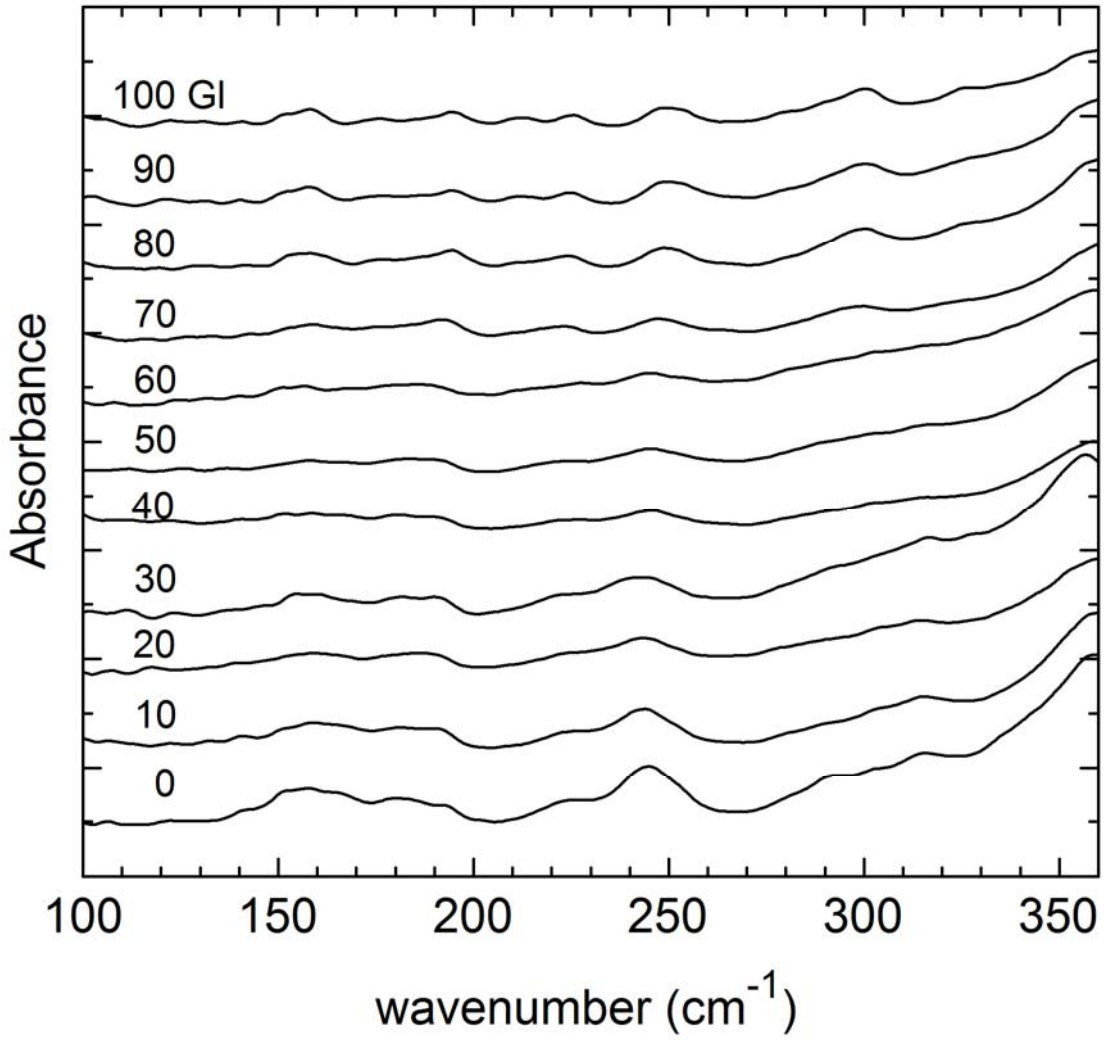

965

966

967

968 Figure 10

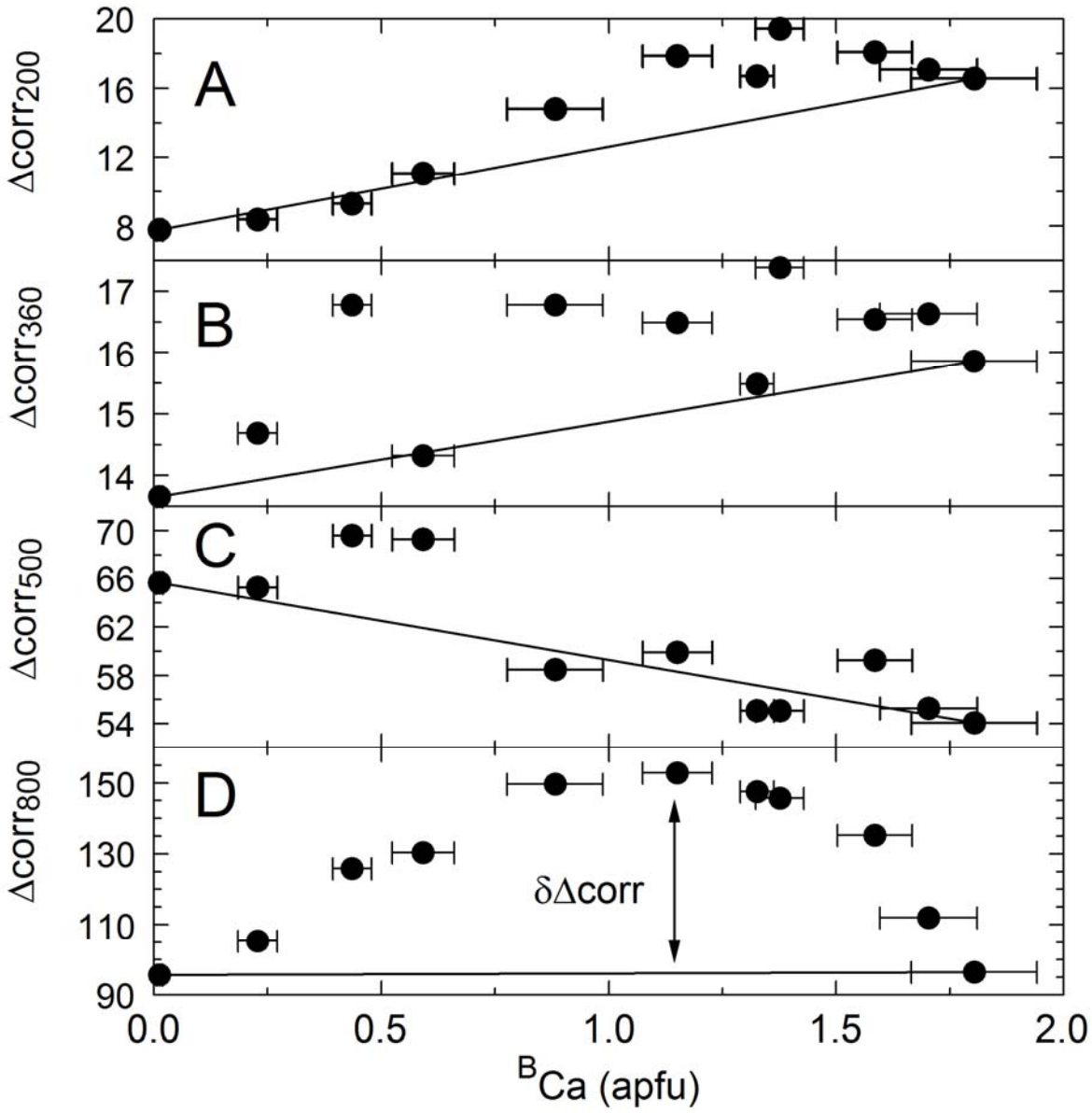

969

970

971 Figure 11

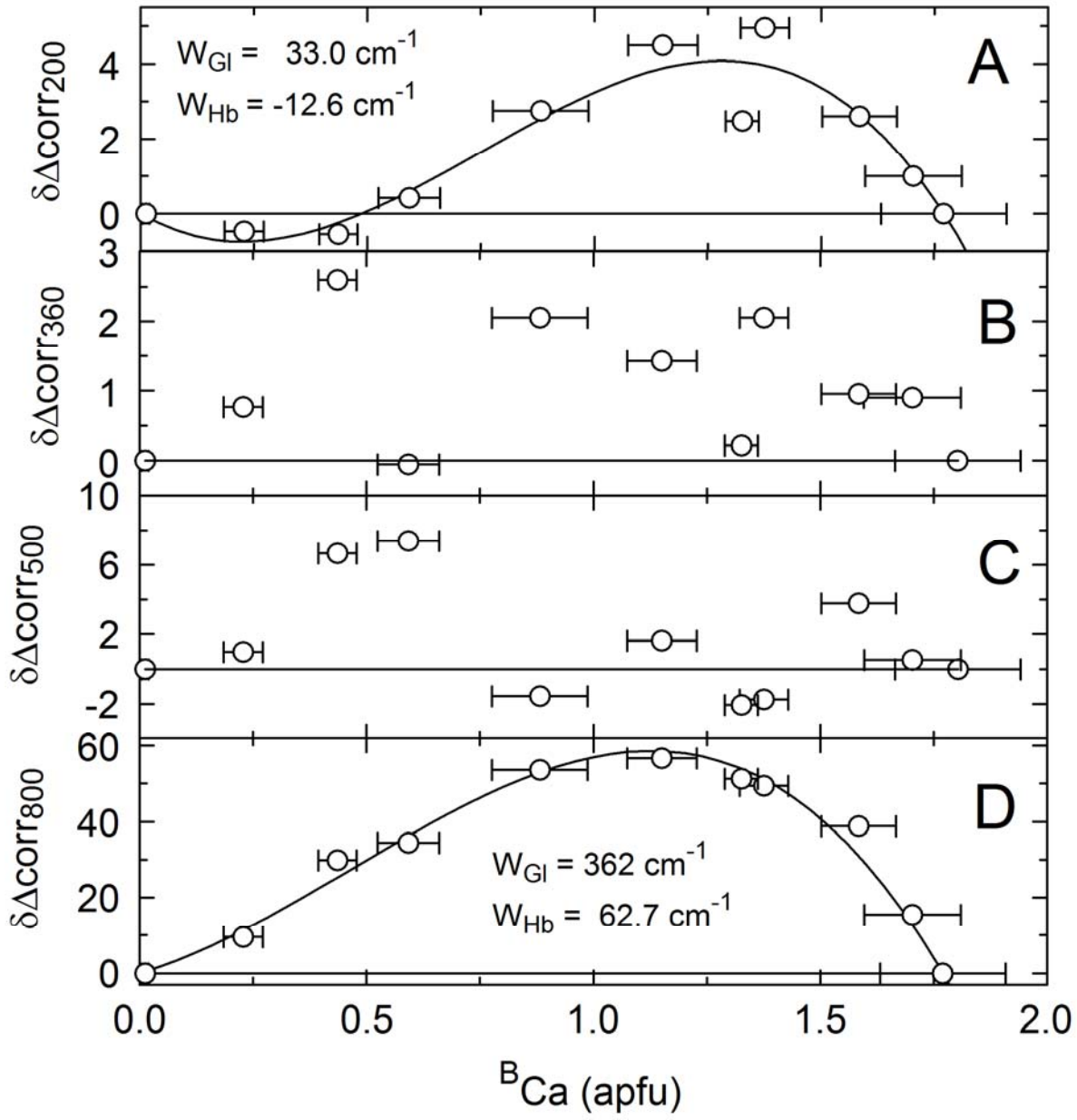

972

973

974 Figure 12.

975

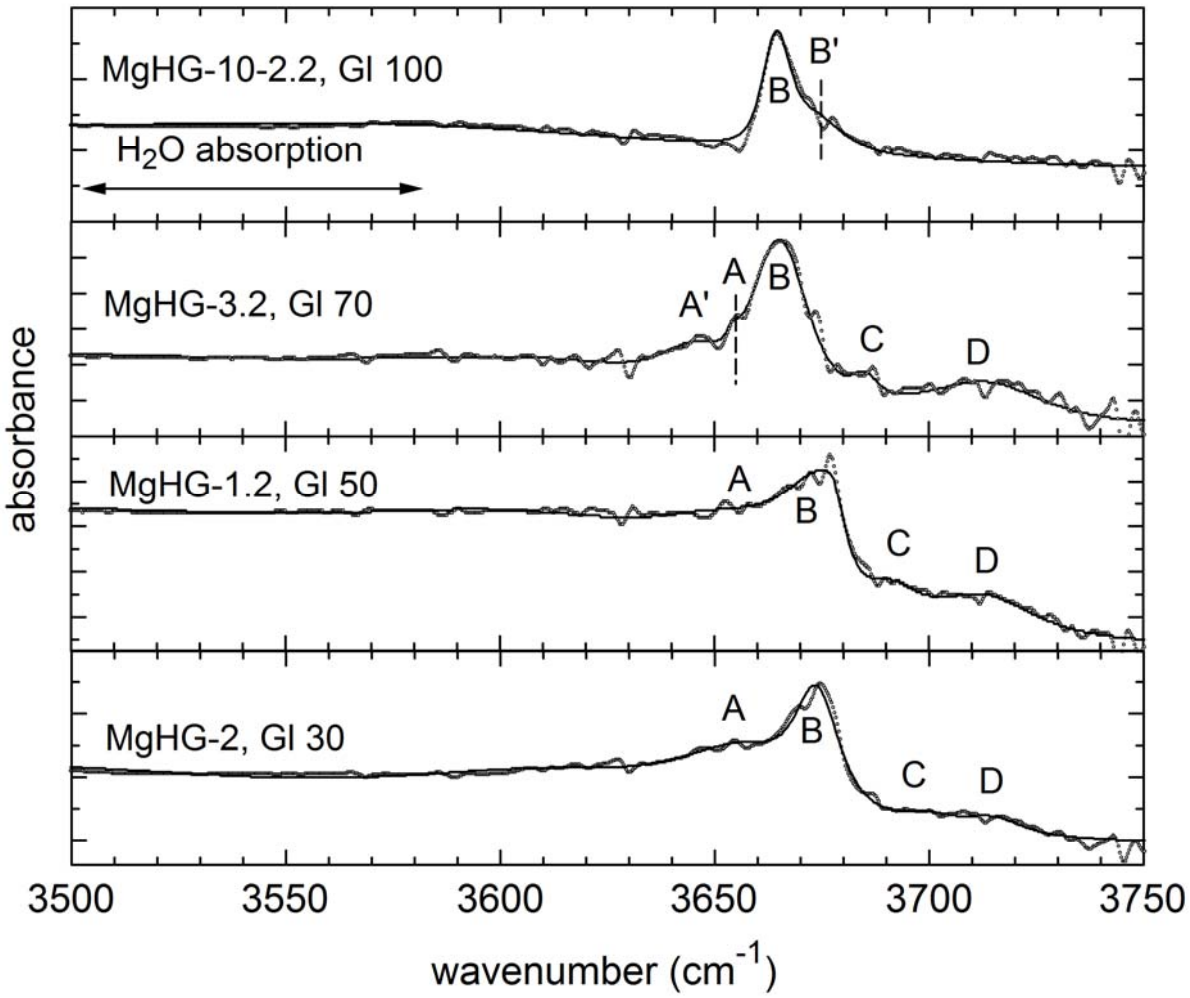

976

977

978 Figure 13.

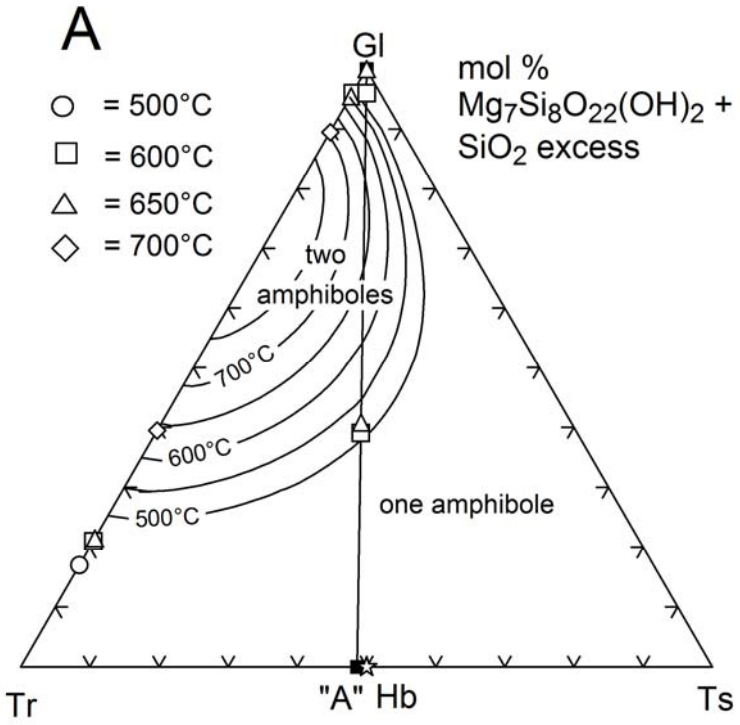

979

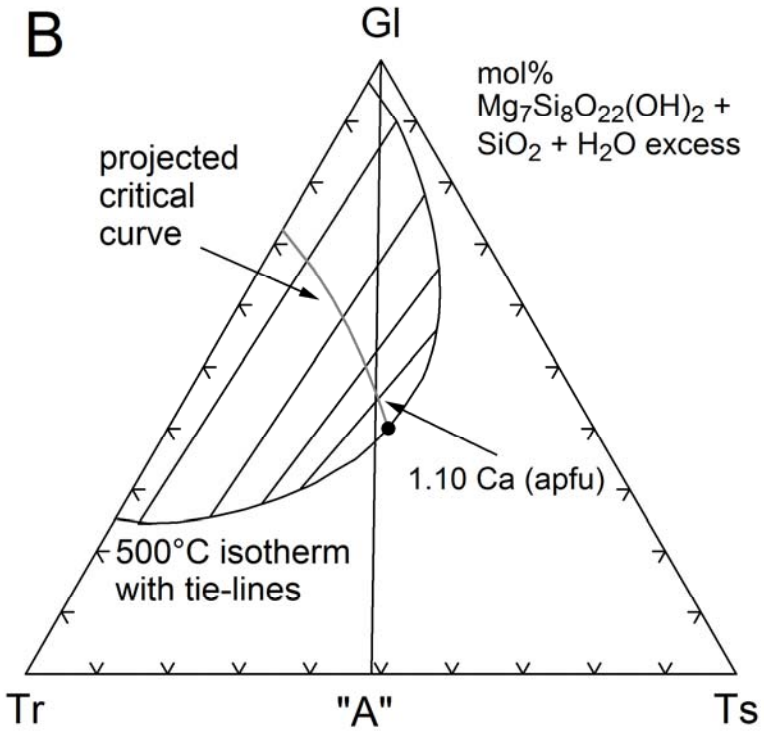

980

981

982 Figure 14

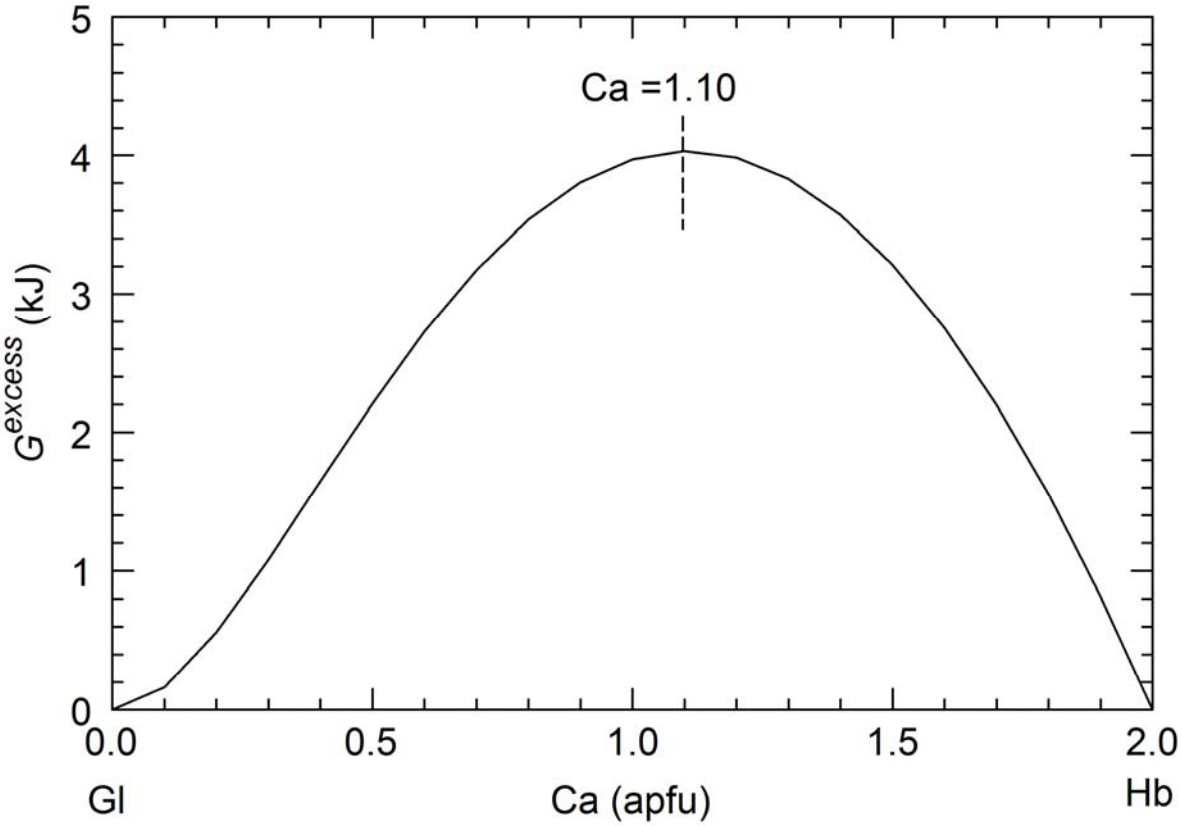

983

984

985

986 Figure 15

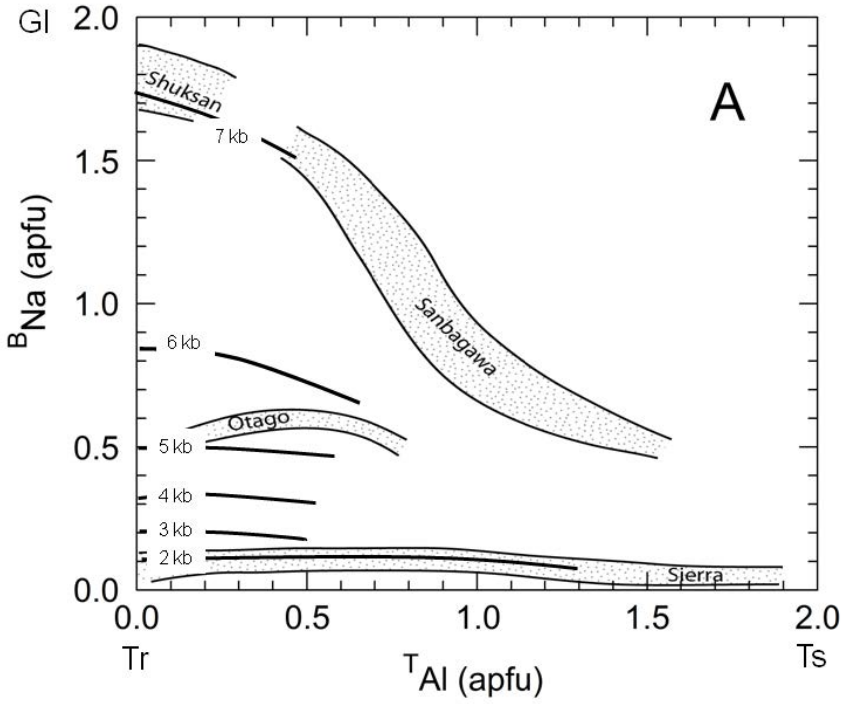

987

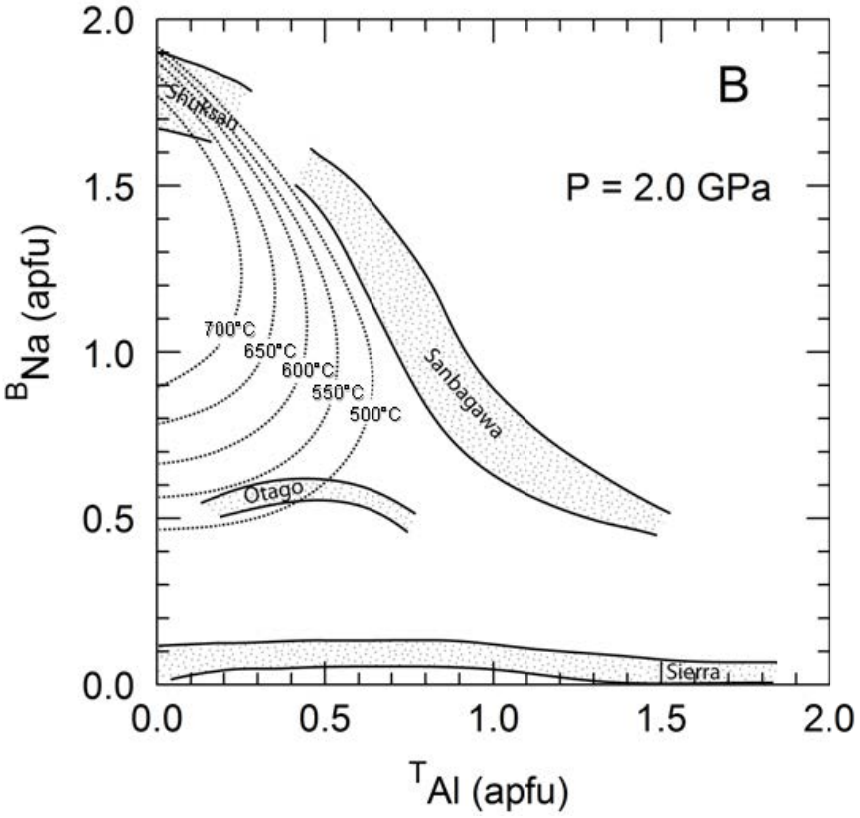

988